# UC Davis UC Davis Previously Published Works

### Title

Excessive Laughter-like Vocalizations, Microcephaly, and Translational Outcomes in the Ube3a Deletion Rat Model of Angelman Syndrome

## Permalink

https://escholarship.org/uc/item/8fz2b3z9

**Journal** Journal of Neuroscience, 41(42)

### ISSN

0270-6474

### Authors

Berg, Elizabeth L Jami, Shekib A Petkova, Stela P et al.

# **Publication Date**

2021-10-20

# DOI

10.1523/jneurosci.0925-21.2021

Peer reviewed



Research Articles: Behavioral/Cognitive

# Excessive laughter-like vocalizations, microcephaly, and translational outcomes in the *Ube3a* deletion rat model of Angelman Syndrome

https://doi.org/10.1523/JNEUROSCI.0925-21.2021

Cite as: J. Neurosci 2021; 10.1523/JNEUROSCI.0925-21.2021

Received: 29 April 2021 Revised: 23 August 2021 Accepted: 26 August 2021

This Early Release article has been peer-reviewed and accepted, but has not been through the composition and copyediting processes. The final version may differ slightly in style or formatting and will contain links to any extended data.

Alerts: Sign up at www.jneurosci.org/alerts to receive customized email alerts when the fully formatted version of this article is published.

Copyright © 2021 Berg et al.

This is an open-access article distributed under the terms of the Creative Commons Attribution 4.0 International license, which permits unrestricted use, distribution and reproduction in any medium provided that the original work is properly attributed.

# Excessive laughter-like vocalizations, microcephaly, and translational outcomes in the *Ube3a* deletion rat model of Angelman Syndrome

Elizabeth L. Berg<sup>1</sup>, Shekib A. Jami<sup>2</sup>, Stela P. Petkova<sup>1</sup>, Annuska Berz<sup>3,4</sup>, Timothy A. Fenton<sup>1</sup>, Jason P. Lerch<sup>5,6,7</sup>, David J. Segal<sup>8</sup>, John A. Gray<sup>2</sup>, Jacob Ellegood<sup>5</sup>, Markus Wöhr<sup>3,4,9,10</sup>, and Jill L. Silverman<sup>1\*</sup>

<sup>1</sup>MIND Institute and Department of Psychiatry and Behavioral Sciences, University of California Davis School of Medicine, Sacramento, CA 95817, USA. <sup>2</sup>Department of Neurology, Center for Neuroscience, University of California Davis, Davis, CA 95618, USA. <sup>3</sup>Behavioral Neuroscience, Experimental and Biological Psychology, Faculty of Psychology, Philipps-University Marburg, 35032 Marburg, Germany. <sup>4</sup>Center for Mind, Brain and Behavior, Philipps-University Marburg, 35032 Marburg, Germany. <sup>5</sup>Mouse Imaging Centre, The Hospital for Sick Children, Toronto, ON M5T 3H7, Canada. <sup>6</sup>Department of Medical Biophysics, University of Toronto, Toronto, ON M5S, Canada. <sup>7</sup>Wellcome Centre for Integrative Neuroimaging, The University of Oxford, Oxford OX3 9DU, UK. <sup>8</sup>MIND Institute, Genome Center, and Department of Biochemistry and Molecular Medicine, University of California Davis, Davis, CA 95616, USA. <sup>9</sup>KU Leuven, Faculty of Psychology and Educational Sciences, Research Unit Brain and Cognition, Laboratory of Biological Psychology, Social and Affective Neuroscience Research Group, B-3000 Leuven, Belgium. <sup>10</sup>KU Leuven, Leuven Brain Institute, B-3000 Leuven, Belgium.

### \*Corresponding Author:

21 Jill L. Silverman

1

2

3 4

5

6 7

8

9

10

11

12 13

14

15

16

17

18

19 20

28 29

30 31

32

33

40

42

- 22 MIND Institute and Department of Psychiatry and Behavioral Sciences
- 23 University of California Davis School of Medicine
- 24 Research II Building 96, 4625 2<sup>nd</sup> Avenue, Suite 1001B
- 25 Sacramento, CA 95817
- 26 Phone: 916-734-8531

27 jsilverman@ucdavis.edu

Running title: USV and AS-relevant outcomes in the Ube3a rat

**Keywords:** Ube3a, Angelman Syndrome, rat model, behavior, ultrasonic vocalizations, play, gait, learning, memory, long term potentiation, MRI.

- 34 Number of pages: 38
- 35 Number of figures: 6
- 36 Number of extended data figures: 2
- 37 Number of words in abstract: 162
- 38 Number of words in introduction: 589
- 39 Number of words in discussion: 1500

41 Conflict of Interest: The authors declare no conflicts of interest.

Acknowledgments: This work was supported by the Foundation for Angelman Syndrome Therapeutics (FAST; ELB, DJS, JLS), the MIND Institute's Intellectual and Developmental Disabilities Resource Center NIH U54HD079125 (JLS; PI LA), the NIMH R01MH117130 (JAG), the Deutsche Forschungsgemeinschaft (DFG WO 1732/4-2; MW), the Canadian Institute for Health Research (CIHR; JPL, JE), the Ontario Brain Institute (OBI; JPL, JE), and the Gustav Adolf Lienert Foundation (AB). The authors thank Matthew Matson, Ruona Lin, Steven Xiong, Yutian Shen, and Anurupa Kar for technical support.

### 50 Abstract

51

52 Angelman Syndrome (AS) is a rare genetic neurodevelopmental disorder characterized by 53 intellectual disabilities, motor and balance deficits, impaired communication, and a happy, excitable 54 demeanor with frequent laughter. We sought to elucidate a preclinical outcome measure in male and 55 female rats that addressed communication abnormalities of AS and other neurodevelopmental disorders in 56 which communication is atypical and/or lack of speech is a core feature. We discovered, and herein report for the first time, excessive laughter-like 50-kHz ultrasonic emissions in the  $Ube3a^{\text{mat-/pat+}}$  rat model of 57 58 AS, which suggests an excitable, playful demeanor and elevated positive affect, similar to the demeanor of individuals with AS. Also in line with the AS phenotype,  $Ube3a^{\text{mat-/pat+}}$  rats demonstrated aberrant 59 60 social interactions with a novel partner, distinctive gait abnormalities, impaired cognition, an underlying 61 long-term potentiation deficit, and profound reductions in brain volume. These unique, robust phenotypes 62 provide advantages compared to currently available mouse models and will be highly valuable as 63 outcome measures in the evaluation of therapies for AS.

64

### 65 Significance Statement

66

67 Angelman Syndrome (AS) is a severe neurogenetic disorder for which there is no cure, despite 68 decades of research using mouse models. This study utilized a recently developed rat model of AS to 69 delineate disease-relevant outcome measures in order to facilitate therapeutic development. We found the 70 rat to be a strong model of AS, offering several advantages over mouse models by exhibiting numerous 71 AS-relevant phenotypes including overabundant laughter-like vocalizations, reduced hippocampal long-72 term potentiation, and volumetric anomalies across the brain. These findings are unconfounded by 73 detrimental motor abilities and background strain, issues plaguing mouse models. This rat model 74 represents an important advancement in the field of AS and the outcome metrics reported herein will be 75 central to the therapeutic pipeline.

### 77 Introduction

78

76

79 Angelman Syndrome (AS) is a rare neurodevelopmental disorder (NDD) characterized by 80 intellectual disability, impaired communication, ataxia, seizures, as well as a happy disposition with a 81 high degree of excitability, smiling, and easily provoked laughter (Williams and Franco, 2010). AS is 82 caused by dysfunction of maternal ubiquitin protein ligase E3A (UBE3A), typically from a de novo 83 deletion in the 15q11-q13 region (Albrecht et al., 1997). Restoring functional UBE3A is seemingly 84 possible by innovative gene therapy approaches including antisense oligonucleotides (Meng et al., 2015), 85 viral vector delivery (Daily et al., 2011), artificial transcription factors (Bailus et al., 2016), stem cell 86 mediated therapies (Adhikari et al., 2021), and the cutting edge Cas9 (Wolter et al., 2020). Gene 87 replacement therapy is therefore on the horizon for AS and, indeed, two clinical trials using "gene 88 therapy-like" antisense oligonucleotide interventions began recruitment in 2020 (GeneTx NCT04259281; 89 Roche NCT04428281).

90 Indispensable to such a strategy of therapeutic development are in vivo studies utilizing 91 preclinical model systems with rigorous translational outcomes. One domain that is critically impaired in 92 AS and other NDDs but difficult to study in preclinical models due to their lack of human-interpretable 93 language is communication. The increasing availability of rat models of NDDs opens up new 94 opportunities to develop preclinical outcome measures of social communication. While the mouse has 95 been the preferred model species in recent decades due to the genetic technologies available, there are 96 complex behaviors and physiological processes difficult or impossible to investigate in mice that are 97 easily observable in rats (Ellenbroek and Youn, 2016; Hofer et al., 2002; Portfors, 2007; Hammerschmidt 98 et al., 2012; Wöhr and Schwarting, 2013; Portfors and Perkel, 2014).

99 One prominent example is the greater sophistication and complexity in the rat acoustic 100 communication system. While both mice and rats emit ultrasonic vocalizations (USV), rats emit USV that 101 serve as situation-dependent, evolved signals which accomplish important communicative functions that 102 are not observed as functions of mouse USV, such as low-frequency 22-kHz "alarm calls" which rats use 103 to warn of potential threats (Brudzynski, 2013; Wöhr and Schwarting, 2013; Blanchard et al., 1991; 104 Sadananda et al., 2008; Fendt et al., 2018; Wöhr and Schwarting, 2007; Kisko et al., 2017). The recent 105 generation of the first rat model of AS therefore provides the unique opportunity to utilize a greater 106 diversity of social and communication behaviors as compared to those previously available in mouse 107 models (Jiang et al., 2010; Huang et al., 2013; Dutta and Crawley, 2020; Kondrakiewicz et al., 2019; 108 Netser et al., 2020; Parker et al., 2014; Ellenbroek and Youn, 2016; Homberg et al., 2017; Reppucci et al., 109 2020).

110 To build upon the initial reports describing the Ube3a deletion rat model of AS, which revealed 111 deficits in motor, cognition, social approach, and pup vocalizations (Berg et al., 2020c; Dodge et al., 112 2020), we sought to investigate nuanced social behaviors and further characterize vocalization patterns. 113 With numerous novel therapies being assessed in clinical trials and at the investigational drug discovery 114 level, AS-relevant outcome measures are vital for demonstrating functional efficacy of the varied 115 intervention approaches. Leveraging the rat's social communication system, we discovered that the Ube3a maternal deletion rat (Ube3a<sup>mat-/pat+</sup>) produces excessive signals of positive affect characteristic of 116 117 AS. Several other AS-relevant phenotypes were evident, including atypical social interactions and 118 maladaptive impairments in gait and cognition. We also identified reduced hippocampal long-term 119 potentiation, observed in mouse models of AS but not yet in rats, as a putative cellular mechanism 120 underlying the learning and memory deficits apparent in the model. Finally, our neuroimaging analysis 121 revealed decreased brain volume and pronounced increasing severity with age.

122

### 123 Materials and Methods

124

Subjects. Subjects were male and female Sprague Dawley Ube3a<sup>mat-/pat+</sup> rats and their wildtype littermates (Ube3a<sup>mat+/pat+</sup>) generated from breeding pairs of paternal Ube3a deletion females and wildtype males purchased from Envigo (Indianapolis, IN). The initial generation of Ube3a deletion rats using

CRISPR/Cas9 was described previously (Berg et al., 2020c). Genotyping was performed using a small 128 129 sample of tail tissue collected at postnatal day (PND) 2, REDExtract-N-Amp (Sigma Aldrich, St. Louis, 130 Rubel123 TAGTGCTGAGGCACTGGTTCAGAGC, Rube1606r MO, USA), and primers 131 TGCAAGGGGTAGCTTACTCATAGC, Ub3aDelSpcfcF6 ACCTAGCCCAAAGCCATCTC, and 132 Ub3aDelR2 GGGAACAGCAAAAGACATGG. All animals were socially housed in a temperature-133 controlled vivarium maintained on a 12:12 light-dark cycle with testing occurring during the light 134 phase. All procedures were conducted in compliance with the NIH Guidelines for the Care and Use of 135 Laboratory Animals and approved by the Institutional Animal Care and Use Committee of the University 136 of California Davis. To minimize the carry-over effects from repeated testing and handling, seven mixed-137 sex cohorts of rats were tested and behavioral tests were carried out in order of least to most stressful with 138 at least 48 hrs break between tests. Each cohort was comprised of four to nine litters and subjects were 139 sampled as followed: subjects for 50-kHz ultrasonic (USV) playback were sampled from Cohort 1; 140 contextual and cued fear conditioning from Cohort 2; gait analysis, heterospecific play, and social play 141 from Cohort 3; acoustic startle and long-term potentiation from Cohort 4; spontaneous exploratory USV 142 from Cohort 5; spontaneous alternation from Cohort 6; and olfactory discrimination from Cohort 7. 143 Following behavioral testing, rats from Cohort 3 were perfused for magnetic resonance imaging.

144

145 Juvenile USV in response to heterospecific play. At postnatal day (PND) 30 through 34, rats 146 were provided daily heterospecific play sessions involving manual stimulation using a slightly 147 abbreviated procedure from those described previously (Burgdorf and Panksepp, 2001; Schwarting et al., 148 2007; Wöhr et al., 2009). For 5 min on 5 consecutive days, rats were individually manipulated by a 149 familiar experimenter using a single clean hand within a clean, empty version of the home cage with fresh 150 bedding (37.2 cm l x 30.8 cm w x 18.7 cm h; illuminated to ~30 lux) while vocalizations were recorded 151 with an overhead ultrasonic microphone (Avisoft Bioacoustics, Glienicke, Germany) for later scoring by 152 a trained observer blinded to genotype. The number of calls emitted during each 30-sec interval were 153 counted and classified as either high (50-kHz) or low (short 22-kHz) frequency using a threshold of 33 154 kHz. Calls emitted during the minute immediately preceding the heterospecific play sessions on days 2-4
155 ("anticipation") were also counted and classified.

156 All rats were handled by the experimenter in a standardized fashion (5 min on 3 days) prior to the 157 first heterospecific play session. The physical manipulations performed were tickling the subject's neck 158 (2x), tickling the subject's belly (1x), pushing into their shoulders ("push and drill"; 1x), and flipping the 159 subject onto their back and momentarily pinning them down ("flip over"; 3x). Each manipulation lasted 160 30 sec with three 30-sec breaks interspersed at 0, 60, and 150 sec, during which the experimenter did not 161 initiate touching the subject but moved their hand around the cage to encourage following or chasing. In 162 an effort to provide a standardized experience, a single experimenter carried out the procedure for all 163 subjects and the experimenter remained unaware of USV being emitted during the test, performing the 164 manipulations in an equivalent manner for all rats. To mitigate any potential effect of order, the sequence 165 of manipulations was re-ordered each day but remained consistent across all animals. The testing order of 166 the subjects was also changed from day to day.

167

Juvenile spontaneous exploratory USV. At PND 30, rats were individually placed in a clean, empty version of the home cage (illuminated to ~30 lux) with clean bedding for 5 min similarly to methods described previously (Schwarting et al., 2007; Wöhr et al., 2008). Recording of ultrasonic vocalizations began immediately following the subject being placed into the cage and no other animals or any experimenter were present in the room during recording. Calls were classified by a trained observer blinded to genotype as either high (50-kHz) or low (short 22-kHz) frequency using a threshold of 33 kHz.

Juvenile USV in response to playback of 50-kHz USV. At PND 30±4, subjects were individually presented with 1-min of natural pro-social 50-kHz USV while on a radial maze illuminated to ~8 lux as described previously (Berg et al., 2018; Berg et al., 2020c). USV were presented to individual subjects using an established playback paradigm (Berg et al., 2018; Wöhr et al., 2016), including the USV stimulus previously demonstrated to elicit social approach (behavior shown in Berg et al., 2020c). The USV stimulus consisted of 221 natural 50-kHz USV recorded from a naïve male rat during exploration of a cage containing a recently separated cage mate. A 3.5-sec sequence of 13 calls was repeated 17 times such that 221 50-kHz calls were presented within 1 min. Response vocalizations were recorded with an overhead ultrasonic microphone (Avisoft Bioacoustics) and the number of calls emitted during the minute of playback were counted by a trained observer blinded to genotype and classified as high (50-kHz) or low (short 22-kHz) frequency using a threshold of 33 kHz.

186

187 Juvenile social play. At PND 38±1, social play behavior was assessed following a protocol 188 described previously (Berg et al., 2018; Berg et al., 2020a; Berg et al., 2020b). Each subject rat was 189 placed with a freely moving, unfamiliar, strain-, sex-, and age-matched wildtype stimulus rat for 10 min 190 in a clean, empty test arena (illuminated to ~30 lux) containing a thin layer of clean bedding. In order to 191 facilitate social play, each subject and stimulus animal was socially isolated in a separate holding room 192 for 30 min prior to the test. Stimulus animals were generated from wildtype Sprague-Dawley breeders 193 (Envigo, Indianapolis, IN) and handled in a standardized manner (5 min on 3 days) prior to the assay. The 194 interaction was video-recorded, and behaviors were later scored by a trained observer blinded to genotype 195 as follows: Social sniffing: sniffing the stimulus rat's face, body, or tail; Anogenital sniffing: sniffing the 196 stimulus rat's anogenital region; Self-grooming: subject grooming itself; Exploring: sitting, walking, 197 rearing, or sniffing the ground or wall; Following or chasing: following (walking pace) or chasing 198 (running pace) the stimulus rat; Rough-and-tumble playing: accelerated movement involving chasing, 199 pouncing, pinning, tumbling, and/or boxing which requires the stimulus rat's participation (i.e., 200 reciprocity); Push past: directed movement toward the stimulus rat to get next to, or move closely past, 201 without sniffing or otherwise engaging; Push under or crawl over: head dip under the stimulus rat's belly 202 or completely stepping over the stimulus rat; Pounce: both paws placed via leap or directed movement 203 onto the stimulus rat's back. Blind scoring was possible since Ube3a<sup>mat-/pat+</sup> rats have normal body weight 204 and are physically indistinguishable from their wildtype littermates (Berg et al., 2020c).

206 **Olfactory discrimination.** At  $42\pm3$ , the ability of rats to discriminate between a social and non-207 social odor was tested by measuring the time spent investigating odor-saturated cotton swabs. Subjects 208 were individually tested in clean chambers (40.6 cm l x 40.6 cm w x 28 cm h) dimly illuminated to ~30 209 lux. On the day before the test, rats were habituated to the test chamber containing a clean dry cotton 210 swab (15.2 cm l) for 20 min. The tip of the swab was secured 3 cm above the floor in the center of the 211 arena by being attached to the top of a clean weighted glass dome (7.6 cm d x 10 cm h) and angled 212 downward. On the day of the test, rats were again habituated to the arena containing a clean dry cotton 213 swab for 10 min, followed by a swab soaked in water, then vanilla (1:100 dilution; McCormick, Hunt 214 Valley, MD), and then a social scent. The social scent was collected by wiping a cotton swab in a zig zag 215 pattern along the bottom of a cage of same sex but unfamiliar Sprague Dawley rats (Envigo, Indianapolis, 216 IN). Each saturated swab was presented for 2 min and the order of odor presentation was consistent across 217 all animals. Time spent sniffing the swab soaked with vanilla scent and the swab soaked with social scent 218 (defined as the nose within 2 cm of the cotton swab tip) was measured using videotracking software 219 (EthoVision XT, Noldus Information Technology, Leesburg, VA), which was subsequently validated 220 manually.

221

Juvenile gait. At PND 25, gait metrics were collected using the DigiGait automated treadmill system and analysis software (Mouse Specifics, Inc., Framingham, MA). Subjects were placed individually into the enclosed treadmill chamber and allowed to acclimate before the belt was turned on. The belt speed was slowly increased to a constant speed of 20 cm/sec, at which each rat was recorded making clearly visible consecutive strides for 3-6 sec.

227

Juvenile contextual and cued fear conditioning. At PND 43±1, learning and memory were assessed using an automated fear conditioning chamber (Med Associates, Inc., Fairfax, VT) following methods previously described (Copping et al., 2017; Adhikari et al., 2018; Berg et al., 2020b). On day one, rats were trained via exposure to a series of three noise-shock (conditioned stimulus-unconditioned stimulus; CS-US; 80 dB white noise, 0.7 mA foot shock) pairings inside a sound-attenuated chamber with specific visual, tactile, and odor cues. On day two, contextual memory was tested by placing each subject back inside the training environment (no noise or foot shock occurred). On day three, cued memory was evaluated by placing subjects into a novel context with altered visual, tactile, and odor cues. Following a period of exploration, the white noise CS was presented for 3 min. Time spent freezing was measured using VideoFreeze software (Med Associates, Inc.).

238

239 Prepulse inhibition of an acoustic startle response. At 9-10 weeks of age, prepulse inhibition 240 was measured using an SR-Lab System (San Diego Instruments, San Diego, CA). Subjects were placed in 241 a clear plastic cylinder, which was mounted onto a platform connected to piezoelectric transducers inside 242 a sound-attenuating chamber with internal speakers. The background noise level in the chamber was 70 243 decibel (dB) white noise. Each session consisted of a 5-min acclimation period followed by a pseudo-244 randomized presentation of 50 trials of five different trial types: one trial type was a 40-ms 120-dB startle 245 stimulus, three trial types involved an acoustic prepulse (74, 82, or 90 dB) presented 120 ms prior to the 246 120-dB startle stimulus, and there were also trials with no startle stimulus in order to measure baseline 247 movement inside the cylinder. Each trial type was presented in 10 blocks and was randomized within 248 blocks. The intertrial interval varied randomly between 10 sec and 20 sec. Percent PPI was calculated 249 using the equation:  $\% PPI = [1 - (Prepulse/Max Startle)] \times 100$ .

250

Spontaneous alternation. At 10 weeks of age, spontaneous alternation was measured by allowing rats to freely explore a novel Y-maze (black, opaque; arms: 21" 1 x 4.5" w x 11" h; illuminated to ~30 lux) for 8 min. An overhead camera connected to videotracking software (EthoVision XT; Noldus Information Technology, Wageningen, Netherlands) was used to quantify the number of arm entries, the number of errors (defined as the sum of direct and indirect revisits to an arm), the number of spontaneous alternations, and the maximum number of possible alternations for the entire session.

258 Long-term potentiation (LTP). Acute slice preparation. At 12-13 weeks of age, subjects were 259 deeply anesthetized with isoflurane and, following decapitation, the brain was rapidly removed and 260 submerged in ice-cold, oxygenated (95% O2/5% CO2) ACSF containing (in mM) as follows: 124 NaCl, 4 261 KCl, 25 NaHCO<sub>3</sub>, 1 NaH<sub>2</sub>PO<sub>4</sub>, 2 CaCl<sub>2</sub>, 1.2 MgSO<sub>4</sub>, and 10 glucose. On an ice-cold plate, the brain 262 hemispheres were separated, blocked, and the hippocampi removed. The 400-umat-thick slices were then 263 cut using a McIlwain tissue chopper (Brinkman, Westbury, NY). Slices from the dorsal thirds of the 264 hippocampus were used. Slices were incubated (at 33°C) for 20 min and then maintained in submerged-265 type chambers that were continuously perfused (2-3 mL/min) with ACSF and allowed to recover for at 266 least 1.5-2 hr before recordings. Just prior to start of experiments slices were transferred to a submersion 267 chamber on an upright Olympus microscope, perfused with 30.4°C normal ACSF saturated with 95% 268 O<sub>2</sub>/5% CO<sub>2</sub>.

269 Electrophysiological recordings. A bipolar, nichrome wire stimulating electrode (MicroProbes) 270 was placed in stratum radiatum of the CA1 region and used to activate Schaffer collateral/commissural 271 fiber synapses. Evoked fEPSPs (basal stimulation rate = 0.033 Hz) were recorded in *stratum radiatum* 272 using borosilicate pipettes (Sutter Instruments, Novato, CA) filled with ACSF (resistance 5-10 m $\Omega$ ). 273 Submerged-type recording chambers were used for all recordings. All recordings were obtained with a 274 MultiClamp 700B amplifier (Molecular Devices, San Jose, CA), filtered at 2 kHz, digitized at 10 Hz. To 275 determine response parameters of excitatory synapses, basal synaptic strength was determined by 276 comparing the amplitudes of presynaptic fiber volleys and postsynaptic fEPSP slopes for responses 277 elicited by different intensities of SC fiber stimulation. Presynaptic neurotransmitter release probability 278 was compared by paired pulse facilitation (PPF) experiments, performed at 25, 50, 100 and 250 msec 279 stimulation intervals. LTP was induced by high frequency stimulation (HFS) using a 2x tetanus (1-s-long 280 train of 100 Hz stimulation) with a 10 sec inter-tetanus interval. At the start of each experiment, the 281 maximal fEPSP amplitude was determined and the intensity of presynaptic fiber stimulation was adjusted 282 to evoke fEPSPs with an amplitude ~40-50% of the maximal amplitude. The average slope of EPSPs 283 elicited 55-60 min after HFS (normalized to baseline) was used for statistical comparisons.

284

285 Magnetic resonance imaging (MRI). At 6.5 months of age, ex vivo neuroimaging was carried 286 out by following a protocol previously described (Berg et al., 2018; Berg et al., 2020c). Brains were 287 flushed and fixed via transcardial perfusion with 50 mL phosphate-buffered saline (PBS) containing 10 288 U/mL heparin and 2 mM ProHance (gadolinium contrast agent; Bracco Diagnostics Inc., Monroe 289 Township, NJ) followed by 50 mL 4% paraformaldehyde in PBS containing 2 mM ProHance. Brains 290 were incubated in the 4% PFA solution at 4°C for 24 hrs, transferred to a 0.02% sodium azide PBS 291 solution, and then incubated at 4°C for at least one month before being scanned. Magnetic resonance 292 imaging (MRI) of the brains within their skulls was carried out using a multi-channel 7.0 Tesla scanner 293 (Agilent Inc., Palo Alto, CA). Seven custom millipede coils were used to image the brains in parallel 294 (Bock et al., 2005; Lerch et al., 2011). Parameters used in the anatomical MRI scans: T2 weighted 3D fast 295 spin echo sequence, with a cylindrical acquisition of k-space, and with a TR of 350 ms, and TEs of 10.5 296 ms per echo for 12 echoes, field of view 36 x 36 x 40 mm<sup>3</sup> and a matrix size of 456 x 456 x 504 giving an 297 image with 0.079 mm isotropic voxels (Noakes et al., 2017). The current scan time for this sequence is  $\sim$ 298 3 hours.

299 To visualize and compare any changes in the rat brains the images were linearly and non-linearly 300 registered together using the pydpiper framework. Registrations were performed using a combination of 301 mni\_autoreg tools (Collins et al., 1994) and ANTS (advanced normalization tools) (Avants et al., 2011). 302 Following registration, a population atlas was created representing the average anatomy of the study 303 sample. At the end of the registration process all the scans were deformed into alignment with one another 304 in an unbiased fashion. This allows for analysis of the deformations required to register the brains 305 together, which can be used to assess the volume of the individual brains and compared them to one 306 another (Bishop et al., 2006; Lerch et al., 2008c; Lerch et al., 2008a; Lerch et al., 2008b; Nieman et al., 307 2010; Nieman et al., 2018). For comparisons to the juvenile brains, a separate registration pipeline was 308 used that included all the brains from this study as well as the previous Berg et al. (2020) study. 309 Volumetric differences were calculated on a regional and a voxelwise basis. An in-house manually

310 segmented hierarchical rat brain atlas was used to calculate the volumes of 52 different segmented 311 structures. These structures were derived from multiple atlases (Dorr et al., 2008; Steadman et al., 2014) 312 and then modified for use in the rat brain.

313

Experimental design and statistical analyses. Statistical analyses were performed using GraphPad Prism 8 statistical software (GraphPad Software, San Diego, CA). Clampex 10.6 software suite (Molecular Devices, San Jose, CA) was used for analyzing electrophysiological data. Congruent with previous studies, no significant sex differences were detected so the results herein include both males and females. Effect sizes and power were determined using Cohen's *d*.

319 Analysis of behavior and LTP. For single comparisons between two groups, either a Student's t-320 test or Mann-Whitney U test was used. Data that passed distribution normality tests, were collected using 321 continuous variables, and had similar variances across groups were analyzed via Student's t-test. 322 Alternatively, a Mann-Whitney U test was used. Either a two-way analysis of variance (ANOVA) or two-323 way repeated measures ANOVA was used to analyze the effects of genotype and a second factor. In 324 repeated measures ANOVA, genotype was the between-group factor and time, limb set, test phase, scent, 325 or prepulse intensity was the within-group factor. Post-hoc comparisons were performed following a 326 significant main effect or interaction and were carried out using Holm-Sidak's multiple comparisons test 327 controlling for multiple comparisons. Data points within two standard deviations of the mean were 328 included, all significance tests were two-tailed, and a p-value of < 0.05 was considered significant.

*Analysis of MRI.* Statistical analyses were used to compare both the absolute and relative volumes voxelwise as well as across the 52 different hierarchical structures in the rat brains. Absolute volume was calculated as mm<sup>3</sup> and relative volume was assessed as a measure of % total brain volume. Voxelwise and regional differences were assessed using linear models. All image analysis tools and software is available on Github (https://github.com/Mouse-Imaging-Centre). Multiple comparisons were controlled for using the False Discovery Rate (Genovese et al., 2002).

### 335

### 336 Results

337

Overabundant emission of laughter-like 50-kHz calls in juvenile Ube3a<sup>mat-/pat+</sup> rats. Since 338 339 deficient expressive communication and elevated rates of positive affect are key clinical features of AS, 340 we sought to quantify these characteristics in  $Ube3a^{mat-/pat+}$  and  $Ube3a^{mat+/pat+}$  (wildtype) rats. While 341 vocalizations are readily collected during social play, recording USV from multiple interacting animals 342 makes it difficult to determine which animal made each call. We therefore took advantage of the fact that 343 rats emit laughter-like 50-kHz calls when social play is simulated by an experimenter via tickling and 344 other physical maneuverings (Burgdorf and Panksepp, 2001; Burgdorf et al., 2005; Burgdorf et al., 2008; 345 Ishiyama and Brecht, 2016). We implemented a standardized heterospecific play procedure (Figure 1A) 346 to elicit USV (Figure 1B) while maintaining full confidence in the identity of the caller and controlling 347 for the level of physical interaction across subjects.

348 We discovered that while both groups increased 50-kHz USV emission across consecutive 349 sessions,  $Ube_3a^{\text{mat-/pat+}}$  emitted a substantially elevated level of 50-kHz USV (Figure 1C; 350  $F_{\text{Genotype}(G)}(1,48)=7.351, p=0.009; F_{\text{Dav}(D)}(3.007,144.3)=10.82, p<0.0001; F_{\text{D}\times\text{G}}(4,192)=1.052, p>0.05).$  In 351 total,  $Ube3a^{\text{mat-/pat+}}$  emitted an average of  $33 \pm 5$  USV per minute (mean  $\pm$  S.E.M.), more than twice the 352 rate of controls, which produced an average of  $15 \pm 3$  calls per minute (Figure 1D; U=175, p=0.007, 353 d=0.77). A closer examination revealed that 50-kHz USV were elevated during the break and belly tickle 354 phases (Figure 1E;  $F_G(1,48)=6.927$ , p=0.011;  $F_{Phase (P)}(1.722,82.64)=27.83$ , p<0.0001;  $F_{P\times G}(4,192)=2.075$ , 355 p > 0.05; post-hoc: break, p = 0.023, d = 0.85; belly tickle, p = 0.023, d = 0.84), although calling during the 356 other phases also trended higher, providing strong evidence of elevated positive affect and a high hedonic 357 impact of the assay (neck tickle, p=0.057, d=0.62; push and drill, p=0.057, d=0.65; flip over, p=0.057, 358 d=0.69). There was no effect of sex, nor an interaction with sex, (p>0.05) for any parameter.

Additionally, 50-kHz USV were more frequently emitted during the anticipation period immediately prior to the play sessions (Figure 1F; U=146.5, p=0.001, d=1.04). In total, across all four anticipation timepoints (days 2-5),  $Ube3a^{\text{mat-/pat+}}$  emitted an average of  $9 \pm 2$  USV per minute (mean  $\pm$ S.E.M.), more than four times the rate of wildtypes, which produced an average of  $2 \pm 0.4$  calls per minute. This indicates that  $Ube3a^{\text{mat-/pat+}}$  predicted the impending onset of play and that the interaction had a high degree of incentive salience.

Excessive vocalization by Ube3a<sup>mat-/pat+</sup> rats was specific to 50-kHz USV. Production of short 22-365 366 kHz USV, which are emitted in modest amounts during play, was low and did not differ between 367 genotypes (Figure 1G;  $F_G(1,48)=1.771$ , p>0.05;  $F_D(1.825,87.62)=3.160$ , p>0.05;  $F_{D\times G}(4,192)=1.330$ , p>0.05). Elevated 50-kHz calling by Ube3a<sup>mat-/pat+</sup> was also specific to being provoked by heterospecific 368 369 play, as 50-kHz and short 22-kHz USV production was normal during exploration of an empty cage 370 (albeit a slight trend toward greater 50-kHz USV; Figure 1H; 50-kHz, U=374.5, p>0.05; 22-kHz, U=433, 371 p>0.05, d=0.56) and in response to the acoustic presentation of 50-kHz USV (Figure 1I; 50-kHz, U=53, 372 p > 0.05; 22-kHz, U = 44.50, p > 0.05). No gross abnormalities in call structure were observed. Specifically, 373 50-kHz calls were of normal duration and peak frequency (Figure 1J: U=205, p>0.05; Figure 1K: U=240, 374 p > 0.05; Figure **1N**: U = 52, p > 0.05; Figure **1O**: t(19) = 0.3179, p > 0.05), suggesting that increased 375 heterospecific play 50-kHz call numbers were not inflated by shorter or broken calls. Duration and peak 376 frequency of 22-kHz USV were also comparable between genotypes (Figure 1L: U=12, p>0.05; Figure 377 1M: t(11)=1.699, p>0.05; Figure 1P: U=1, p>0.05; Figure 1Q: U=1, p>0.05). Since the average duration 378 of the juvenile 22-kHz USV fell short of the usual durations of adult "typical 22-kHz" USV, we herein 379 refer to them as "short 22-kHz" USV.

380

Intact social interest but deficient expression of key social interaction behaviors in juvenile Ube3a<sup>mat-/pat+</sup> rats. We sought to investigate whether elevated 50-kHz USV emission in Ube3a<sup>mat-/pat+</sup> rats was associated with greater social engagement with a conspecific. Starting around two weeks of age, rats play fight with each other by chasing, pouncing, pinning, and wrestling in a manner similar to cats and dogs. Through developmental experience, they learn how to appropriately initiate, engage in, and terminate play bouts with others. In order to more closely examine social behavior and the nuanced 387 reciprocal interactions of social play, we gave juvenile subjects the opportunity to freely interact with a 388 conspecific (Panksepp, 1981). Despite greater 50-kHz calling during heterospecific play, Ube3a<sup>mat-/pat+</sup> rats 389 showed a normal degree of interest in the stimulus animal, demonstrated by the amounts of time spent 390 social sniffing (Figure 2A; t(20)=1.646, p>0.05) and anogenital sniffing (Figure 2B; t(20)=0.4457, 391 p > 0.05). Putting forth a similar level of investigative effort suggested that  $Ube3a^{\text{mat-/pat+}}$  are just as 392 motivated for social interaction as controls. Levels of self-grooming (Figure 2C; U=38, p>0.05) and arena exploration (Figure 2D; U=30, p>0.05) were also normal but Ube3a<sup>mat-/pat+</sup> spent markedly less time 393 394 following or chasing the stimulus rat (Figure 2E; U=29, p=0.041, d=1.11). The key observation was the 395 reduced time spent rough-and-tumble playing (Figure 2F; U=33.50, p=0.029, d=0.89) compared to 396 wildtypes. In an attempt to reconcile the near lack of play with intact levels of social interest, we 397 quantified specific components of rough-and-tumble play. While the number of side-to-side social 398 contacts via push pasts were similar across genotypes (Figure 2G; t(20)=0.3852, p>0.05), there was a 399 trending reduction in the number of push under or crawl overs (Figure 2H; U=31.5, p=0.061, d=0.89) and 400 almost a complete lack of pouncing in  $Ube3a^{\text{mat-/pat+}}$  (Figure 2I; U=24, p=0.008, d=1.14). A separate test 401 of olfaction was used to rule out an olfactory deficit as a confounder of social investigation (Figure 2J; 402  $F_{\text{Genotype}(G)}(1,12)=0.0066, p=0.937; F_{\text{Scent}(S)}(1,12)=14.20, p=0.003; F_{S\times G}(1,12)=0.0165, p=0.900; post-hoc:$ 403 mat+/pat+, *p*=0.035; mat-/pat+, *p*=0.035).

404

Abnormal gait in Ube3a<sup>mat-/pat+</sup> rats. In an effort to assess the potential contribution of motor 405 406 defects to social play behavior, we explored motor dysfunction, which is a core clinical feature of AS 407 prevalent in mouse models (Huang et al., 2013; Leach and Crawley, 2018; Copping and Silverman, 2020) 408 and hypothesized by our group to underlie the open field, rotarod, and marble burying phenotypes of AS mouse models. Previously, we discovered lower open field vertical activity in  $Ube3a^{\text{mat-/pat+}}$  rats while 409 410 other activity indices were typical (Berg et al., 2020c). Using the DigiGait automated treadmill system, 411 we found that juvenile Ube3a<sup>mat-/pat+</sup> rats displayed robust abnormalities in limb propulsion time, 412 indicating reduced limb strength and less force produced per unit time compared to wildtypes (Figure 3A;

413	$F_{\text{Genotype}(G)}(1,44) = 0.0684, \ p > 0.05; \ F_{\text{Limbs}(L)}(1,44) = 776.8, \ p < 0.0001; \ F_{\text{L}\times\text{G}}(1,44) = 12.80, \ p < 0.001; \ post-hoc:$
414	forelimbs, $p=0.030$ , $d=0.60$ ; hindlimbs, $p=0.022$ , $d=0.85$ ; Figure <b>3B</b> ; $F_{G}(1,44)=1.012$ , $p>0.05$ ,
415	$F_{L}(1,44)=687.0, p<0.0001; F_{L\times G}(1,44)=9.391, p=0.004; post-hoc: forelimbs, p=0.010, d=0.65).$ No
416	abnormalities in swing time (Figure 3C; $F_{G}(1,44)=0.1209$ , $p>0.05$ , $F_{L}(1,44)=22.62$ , $p<0.0001$ ;
417	$F_{L\times G}(1,44)=0.2552, p>0.05)$ or total stride time (Figure <b>3D</b> ; $F_G(1,44)=0.9166, p>0.05; F_L(1,44)=13.24,$
418	$p < 0.001$ ; $F_{L\times G}(1,44)=0.7566$ , $p > 0.05$ ) were discovered, suggesting that the opposing effects of propulsion
419	and brake time canceled each other out. Stride length was normal, which was surprising given the
420	published Zeno walkway data in humans (Grieco et al., 2018), but lends to the hypothesis that Ube3a <sup>mat-</sup>
421	$^{/\text{pat}^+}$ have limb weakness since more time was required to produce force for an equal length step (Figure
422	<b>3F</b> ; $F_{\rm G}(1,44)=0.9460$ , $p>0.05$ ; $F_{\rm L}(1,44)=12.70$ , $p<0.001$ ; $F_{\rm L\times G}(1,44)=0.7719$ , $p>0.05$ ). Forelimb stance
423	width was reduced (Figure <b>3G</b> ; $F_{\rm G}(1,44)$ =1.605, $p$ >0.05; $F_{\rm L}(1,44)$ =939.0, $p$ <0.0001; $F_{\rm L×G}(1,44)$ =12.46;
424	post-hoc: forelimbs, $p=0.022$ , $d=0.69$ ) while an elevated forelimb paw angle indicated greater degree of
425	external rotation and splaying (Figure <b>3H</b> ; $F_{G}(1,44)=5.957$ , $p=0.019$ ; $F_{L}(1,44)=3.726$ , $p>0.05$ ;
426	$F_{L\times G}(1,44)=3.497$ , $p>0.05$ ; post-hoc: forelimbs, $p=0.006$ , $d=0.86$ ), which has been associated with ataxia,
427	spinal cord injury, and demyelinating disease (Powell et al., 1999). The observed effects were not
428	attributable to differences in body length (data not shown; $U=244.5$ , $p>0.05$ ) or body width (data not
429	shown; $t(44)=0.2719$ , $p>0.05$ ) and, despite abnormalities in some temporal and postural components of
430	gait, the coordination metric of gait symmetry was unaltered (Figure 3I; $t(44)=1.023$ , $p>0.05$ ).

431

432 Impaired learning and memory in *Ube3a*<sup>mat-/pat+</sup> rats. Learning and memory impairments, 433 which are characteristic of AS, may hinder the ability of *Ube3a*<sup>mat-/pat+</sup> rats to learn via developmental 434 experience how to appropriately engage in social interactions. We therefore probed for a juvenile learning 435 and memory deficit using a fear conditioning assay previously used to detect a deficit in adulthood 436 (Dodge et al., 2020). Following successful fear conditioning (Figure **4A**;  $F_{Phase(P)}(1,30)=48.47$ , p<0.0001; 437  $F_{Genotype(G)}(1,30)=0.2203$ , p>0.05;  $F_{P\times G}(1,30)=0.0613$ , p>0.05; *post-hoc*: mat+/pat+, p<0.0001; mat-/pat+, 438 p<0.001), juvenile *Ube3a*<sup>mat-/pat+</sup> displayed normal levels of freezing in response to the training context 439 (Figure 4B; U=117.5, p>0.05) but a robust deficit in cued fear memory 48 hrs after training (Figure 4C;  $F_{G}(1,30)=7.395$ , p=0.011;  $F_{P}(1,30)=42.36$ , p<0.0001;  $F_{P\times G}(1,30)=8.699$ , p=0.006; post-hoc: pre-cue, 440 441 p > 0.05; cue, p < 0.001, d=1.10). We assessed the potentially confounding variable of impaired 442 sensorimotor processing by measuring the startle response to an intense acoustic stimulus and quantifying 443 the reduction in startle response following prepulses of varying intensities. Both baseline activity (Figure 444 **4D**; t(22)=1.735, p>0.05) and the acoustic startle response of  $Ube3a^{\text{mat-/pat+}}$  rats were normal (Figure **4E**; 445 t(22)=1.157, p>0.05), illustrating intact hearing abilities. While there was a significant main effect of 446 genotype on prepulse inhibition, indicative of a sensorimotor gating deficit ( $F_{\text{Genotype}(G)}(1,22)=4.740$ , 447  $p=0.041, d=0.88; F_{\text{Prepulse}(P)}(1.898,41.75)=20.64, p<0.0001; F_{P\times G}(2,44)=2.127, p=0.1312), post-hoc testing$ 448 revealed no significant difference between groups at any individual prepulse level (Figure 4F; 74 dB, 449 *p*>0.05, *d*=0.25; 82 dB, *p*>0.05, *d*=0.73; 90 dB, *p*>0.05, *d*=1.05).

As an additional assessment of cognitive functioning, we quantified spontaneous alternation during exploration of a Y-maze and found that  $Ube3a^{\text{mat-/pat+}}$  rats displayed reduced spontaneous alternation compared to wildtypes (Figure **4G**; t(46)=3.115, p<0.01, d=0.90).  $Ube3a^{\text{mat-/pat+}}$  rats made 40% more errors (Figure **4H**; t(46)=3.827, p<0.001, d=1.10) and more arm entries (Figure **4I**; t(46)=3.620, p<0.001, d=1.04) despite no difference in the total distance moved (data not shown; Student's *t*-test: t(46)=1.721, p>0.05). Taken together, these metrics indicate additional cognitive deficits in the  $Ube3a^{\text{mat-}}$ (pat+ rats that were not confounded by a locomotor deficiency.

457

**Reduced hippocampal long-term potentiation (LTP) in** *Ube3a*<sup>mat-/pat+</sup> **rats.** To elucidate the neurobiology underpinning the learning and memory deficits of *Ube3a*<sup>mat-/pat+</sup> rats, we quantified longterm potentiation (LTP). Previous studies in mouse models of AS have shown that LTP, a major cellular mechanism underlying learning and memory (Collingridge and Isaac, 2003), is impaired (Jiang et al., 1998; van Woerden et al., 2007; Daily et al., 2011). Here, we examined hippocampal LTP in adult *Ube3a*<sup>mat-/pat+</sup> rats compared to wildtype littermate controls. Since we found hippocampal-dependent contextual fear memory intact at the juvenile age, but a previous report detected a clear deficit in adults 465 (Dodge et al., 2020), we measured hippocampal LTP in adulthood. Basal synaptic strength (Figure 5A; 466  $F_{\text{Genotype}(G)}(1,92)=0.2013, p>0.05; F_{\text{Amplitude}(A)}(5,111)=94.04, p<0.0001; F_{G\times A}(5,92)=0.4107, p>0.05)$  and 467 paired-pulse ratio (Figure **5B**;  $F_G(1,56)=0.065$ , p>0.05;  $F_{Interval(1)}(3,76)=20.96$ , p<0.0001;  $F_{G\times}(3,56)=0.0758$ , p>0.05) were unaltered in Ube3a<sup>mat-/pat+</sup> rats, suggesting no change in baseline 468 469 excitatory transmission. However, consistent with the mouse models of AS (Jiang et al., 1998; van 470 Woerden et al., 2007; Daily et al., 2011), we found that the magnitude of LTP was reduced in Ube3a<sup>mat-</sup> 471  $^{\text{/pat+}}$  rats (Figure 5C and 5D; t(25)=4.641, p<0.0001, d=1.78), suggesting a putative mechanism underlying 472 impairment of learning and memory (Zucker, 1989; Jiang et al., 1998; Zucker and Regehr, 2002; van 473 Woerden et al., 2007; Daily et al., 2011).

474

475 Neuroanatomical pathology in Ube3a<sup>mat-/pat+</sup> rats revealed by high-resolution magnetic 476 resonance imaging (MRI). MRI revealed striking differences in total brain volume at 6.5 months of age, which was decreased by 6.0% in Ube3a<sup>mat-/pat+</sup> rats (q=0.04, Figure 6, Figure 6-1). The overall brain 477 478 volume difference was driven by decreases in the hippocampal region (-6.3%, q=0.04), brain stem (-479 5.6%, q=0.04), thalamus (-7.7%, q=0.01), cerebellum (-9.0%, q=0.02), and deep cerebellar nuclei (-480 12.3%, q=0.0001). Additional differences were found throughout the white matter fiber tracts (-7.6%, 481 q=0.02), including but not limited to the cerebral peduncle (-7.6%, q=0.02), internal capsule (-8.4%, 482 q=0.02), and arbor vita of the cerebellum (-11.7%, q=0.0004). Moreover, trends were seen in other large 483 white matter structures including the corpus callosum (-6.7%, q=0.06) and fornix system (-6.0%, q=0.09). 484 A complete list of the regional structural differences in both absolute (mm<sup>3</sup>) and relative (% total brain) 485 volume is provided in Figure 6-1.

As we had previously examined  $Ube3a^{mat-/pat+}$  rats at a juvenile age (postnatal day (PND) 21) (Berg et al., 2020c), we felt an age by genotype comparison was warranted. Figure 6 highlights these changes in eight coronal slices, separately from both the previous work on juvenile rats and from the current data on adults. A combined dataset using both the juvenile and adult data was then used to examine a genotype by age interaction model, which revealed several regions to diverge with age and 491 genotype: total brain volume (q=0.048), caudoputamen (q=0.03), white matter fiber tracts (q=0.03; Figure **6A**;  $F_{Age(A)}(1,97)=546.5$ , p<0.0001;  $F_{Genotype(G)}(1,97)=11.87$ , p<0.001;  $F_{A\times G}(1,97)=10.68$ , p=0.002; post-492 493 *hoc*: juvenile, p > 0.05; adult, p < 0.0001, d=1.02), hypothalamus (q=0.046; Figure **6B**;  $F_A(1,97)=460.2$ , 494  $p < 0.0001; F_G(1,97) = 5.081, p = 0.026; F_{A \times G}(1,97) = 8.760, p = 0.004; post-hoc: juvenile, p > 0.05; adult, p = 0.026; r_{A \times G}(1,97) = 8.760, p = 0.004; p$ 495 p=0.001, d=0.82), hippocampal region (q=0.046; Figure **6C**;  $F_A(1,97)=434.4, p<0.0001; F_G(1,97)=10.89$ , 496  $p=0.001; F_{A\times G}(1,97)=8.760, p=0.004; post-hoc:$  juvenile, p>0.05; adult, p<0.0001, d=1.02), and thalamus 497 (q=0.02; Figure **6D**;  $F_A(1,97)$ =430.2, p<0.0001;  $F_G(1,97)$ =11.14, p=0.001;  $F_{A\times G}(1,97)$ =14.96, p<0.001; 498 *post-hoc*: juvenile, p > 0.05; adult, p < 0.0001, d=1.22). A full list of the regional genotype by age 499 interactions is located in Figure 6-2. Voxelwise changes were also found throughout the brain of adult Ube3a<sup>mat-/pat+</sup> rats compared to the juvenile age. The changes in the adults were substantially larger, 500 501 signaling a more severe neuroanatomical phenotype with age (Figure 6).

502

### 503 Discussion

504

505 Indispensable to therapeutic development are *in vivo* studies utilizing preclinical model systems. 506 While mice have prevailed as the animal model of AS in recent decades (Jiang et al., 1998), the Ube3a<sup>mat-</sup> 507 <sup>/pat+</sup> rat offers a unique and suitable system for investigating certain complexities of the human AS 508 phenotype, particularly social communication and affect (Brudzynski, 2013; Wöhr and Schwarting, 2013; 509 Burgdorf et al., 2020; Burke et al., 2017; Homberg et al., 2017; Netser et al., 2020). Our discovery of 510 excessive laughter-like 50-kHz USV is the first report of this affective outcome measure in a model of 511 AS, mirroring the affected population. Moreover, reduced social play, atypical gait, impaired cognition, 512 and anatomical and cellular physiology anomalies were easily detected in this model.

We leveraged our model species to discover that *Ube3a*<sup>mat-/pat+</sup> rats produced an overabundance of 50-kHz vocalizations, which reflect a positive affective state and have been referred to as rat laughter (Panksepp and Burgdorf, 2000; Panksepp, 2005), as well as a trend of elevated laughter-like 50-kHz USV without provocation. Excessive 50-kHz USV, suggestive of enhanced 'wanting' and 'liking' the 517 interaction (Berridge, 2009; Berridge and Aldridge, 2009; Berridge et al., 2009; Okabe et al., 2021),
518 closely aligns with the AS profile of a happy disposition and easily provoked laughter. To our knowledge,
519 this is the first report of this method being used in a genetic rat model of a neurological disorder.

520 Exaggerated 50-kHz calling could suggest enhanced effort to elicit social interaction or may be 521 unrelated to the social component of heterospecific play, potentially a neurobiological consequence of a 522 disinhibited vocal production pathway. AS is typified by laughter that is easily provoked regardless of 523 stimuli valence. The phenotype may also reflect enhanced sensitivity to tactile stimulation. Deriving 524 greater reward from physical interactions could explain typical levels of social investigation in the 525 reciprocal interaction test but reduced social approach in three-chambered and USV playback assays, as 526 well as the disinhibition of social interactions in the clinical population. One limitation of our USV 527 analysis was the lack of acoustic feature quantification for the calls evoked by heterospecific play. We 528 did, however, subsequently carry out this analysis for all other USV assays and found no genotype effect 529 on call features.

530 Juvenile social play is a critical way that rats develop social competence and learn how to 531 appropriately engage and communicate with others, analogous to play in young children (Hofer and Shair, 532 1978; Panksepp and Beatty, 1980; Panksepp, 1981; Brudzynski, 2009, 2013; Argue and McCarthy, 2015). 533 Ube3a<sup>mat-/pat+</sup> rats were interested in a novel partner but did not engage in rough-and-tumble play 534 behaviors characteristic of the species, albeit specific to sex and strain. Our finding of no sex difference in 535 rough-and-tumble play aligns with previous reports which also used pre-test social isolation to motivate 536 the subjects to play (Veenema et al., 2013; Bredewold et al., 2014; Bredewold et al., 2015; Reppucci et 537 al., 2018; Kisko et al., 2020). In contrast with studies on mouse models of AS using the three-chambered 538 social approach task (Jamal et al., 2017; Kumar et al., 2019; Perrino et al., 2020; Dutta and Crawley, 539 2020), which have reported contradictory social deficits and "hypersociability," the rat model displayed a 540 typical level of social investigation.

541 Movement disorders (Wheeler et al., 2017) are a hallmark feature of AS, with gait ataxia being 542 one of the most common issues. While the deficits of  $Ube3a^{\text{mat-/pat+}}$  rats were not obvious to the eye, subtle aberrations in stance and paw placement, paired with abnormal braking and propelling, reflect impaired motor coordination. All of this evidence suggests that altered postures affect motor dynamics which results in the gait patterns exhibited by AS individuals and  $Ube3a^{mat-/pat+}$  rats. The limb weakness indicated by our gait analysis aligns with the reduced rearing previously observed (Berg et al., 2020c).

547 We discovered and report for the first time, to our knowledge, of long-term potentiation (LTP) 548 deficits in this rat model (Jiang et al., 1998; Weeber et al., 2003; van Woerden et al., 2007; Filonova et al., 549 2014; Ciarlone et al., 2016), which provides a putative cellular signaling mechanism underlying the 550 learning and memory impairments reported herein and previously (Berg et al., 2020c; Dodge et al., 2020). Juvenile Ube3a<sup>mat-/pat+</sup> rats exhibited deficits in cued fear memory 48 hours post-training, which extends 551 552 the previous finding by Dodge et al. of deficient contextual and cued fear conditioning in adults 72 hours 553 post-training (Dodge et al., 2020). We ruled out impaired sensorimotor abilities as a confounding variable 554 since the acoustic startle response was unaffected.

555 Pronounced deficits in adulthood are supported by neuroimaging. Previously, we discovered a 556 variety of trending volumetric abnormalities at PND 21 (Berg et al., 2020c), however, these new data 557 show more substantial reductions in adults throughout the brain, highlighting a more severe 558 neuroanatomical phenotype with age. Reduced total brain volume may indicate a loss of cellular volume 559 or dendritic complexity over time, and the drastic volume loss in fiber tracts could indicate a loss in 560 axonal numbers, axonal volume, or myelination. In a mouse model of AS, white matter loss was found to 561 play a large role in the overall microcephaly observed (Judson et al., 2017), with an 11% loss in the 562 corpus callosum making it the most affected white matter structure. Ube3a<sup>mat-/pat+</sup> rats showed a trend 563 towards reduced corpus callosum volume (-6.7%), but the largest white matter deficits were cerebellar. In 564 alignment with Judson et al.'s (2017) study in mice, the reduced fiber tracts volume was also 565 disproportionate to the overall brain volume loss, confirming that white matter development plays the 566 major role in the impaired brain growth in AS. Additionally, the 9% decrease in cerebellum size was 567 consistent with cortical loss (-9%), but there was a disproportionate reduction in arbor vitae and deep 568 cerebellar nuclei volume, indicating that the outputs of the cerebellum are impaired.

569 GABAergic neuron loss (Judson et al., 2016) and decreased tonic inhibition in cerebellar granule 570 cells (Egawa et al., 2012) underlie the theory of brain dysfunction in AS, and hypotheses addressing the 571 theory of reduced inhibitory tone are being pursued for small molecule development (Ciarlone et al., 572 2017). The present results are congruent with this overarching mechanism theory of AS, loss of inhibitory 573 tone. Emission of 50-kHz USV induced by heterospecific play is associated with dopamine release in the 574 nucleus accumbens/ventral striatum. These calls have been considered as "joy," "euphoria," and 575 "laughter," supported by behavioral pharmacology showing increased 50-kHz USV resulting from 576 amphetamine administration (Brudzynski, 2013, 2015; Wöhr, 2021). Both vocalizations and gait require 577 fine motor control and thus striatal and motivational components support aberrant frontal-striatal 578 circuitry. Interestingly, the ventral striatum and "reward" associated substrates of the basal ganglia have 579 inhibitory projections, in line with overall theories of AS regarding inhibitory loss.

580 While gross and fine movement are complicated multi-system physiological processes, AS 581 individuals show ataxic movements in both upper and lower limbs and aberrant gait, suggesting the 582 particular involvement of the cerebellum. This was corroborated here and in earlier work by the large 583 reductions in cerebellar nuclei size, which is consistent with our overarching mechanistic hypothesis since 584 Purkinje cell neurons to the deep cerebellar nuclei modulate excitation via inhibition and Egawa et al. 585 (2012) highlighted decreased cerebellar granule cells in AS. Utilizing conditional Ube3a mouse models to 586 identify the neural substrates of circuit hyperexcitability in AS, Judson et al. (2016) provided compelling 587 evidence that GABAergic, but not glutamatergic, Ube3a loss is responsible for mediating the EEG 588 abnormalities and seizures of AS. Previously, we reproduced and extended Judson et al.'s. (2016) data 589 (Copping and Silverman, 2021) and our hypothesis is that this mechanism extends to social 590 communication, cognitive phenotypes, and impaired gait outcomes, as each shares components of 591 learning and motivation. The loss of brain volume in regions dense with inhibitory neurons seen herein 592 provides further corroborative evidence that GABAergic tone underlies functional outcomes. Independent 593 corroboration comes from ErbB inhibitors, which have been reported to reverse LTP deficits in AS model 594 mice (Kaphzan et al., 2012). While glutamate receptor expression and function were unaltered in Ube3a

mice (Kaphzan et al., 2012; Judson et al., 2016), ErbB signaling was shown to rescue LTP impairments in
 *Ube3a* mice via an increase in inhibitory synaptic transmission, corroborating our core overarching
 mechanism of reduced inhibitory tone.

In conclusion, we discovered that Ube3a<sup>mat-/pat+</sup> rats exhibited interest in a social partner but 598 599 expressed an atypically high level of laughter-like vocalizations. Deficits in other AS-relevant domains 600 were also discovered, including gait and cognition, and reduced hippocampal LTP. Future lines of 601 investigation will assess the circuitry and mechanisms underlying the excessive laughter-like USV and 602 social-cognitive anomalies in USV reception, in addition to pursuing other neurobiological endpoints. 603 Overall, our results indicate that the deletion of maternal Ube3a in the rat creates a sophisticated rodent 604 model with high face validity to the human AS phenotype. In the pursuit of effective therapeutics, it is 605 essential to be equipped with a diverse set of behavioral outcome measures and neurological biomarkers by which to assess efficacy. Taken together, we demonstrate that the Ube3a<sup>mat-/pat+</sup> rat offers numerous 606 607 potential outcome measures that are detectable throughout the lifespan.

608

### 609 References

Adhikari, Copping NA, Beegle, Cameron DL, Deng P, O'Geen H, Segal DJ, Fink KD, Silverman JL, JS
 A (2021) Functional rescue in an Angelman syndrome model following treatment with lentivector
 transduced hematopoietic stem cells. Human Molecular Genetics In press.

Adhikari A, Copping NA, Onaga B, Pride MC, Coulson RL, Yang M, Yasui DH, LaSalle JM, Silverman
JL (2018) Cognitive Deficits in the Snord116 Deletion Mouse Model for Prader-Willi Syndrome.
Neurobiol Learn Mem.

Albrecht U, Sutcliffe JS, Cattanach BM, Beechey CV, Armstrong D, Eichele G, Beaudet AL (1997)
Imprinted expression of the murine Angelman syndrome gene, Ube3a, in hippocampal and
Purkinje neurons. Nat Genet 17:75-78.

Argue KJ, McCarthy MM (2015) Utilization of same- vs. mixed-sex dyads impacts the observation of sex
differences in juvenile social play behavior. Curr Neurobiol 6:17-23.

621 Avants BB, Tustison NJ, Song G, Cook PA, Klein A, Gee JC (2011) A reproducible evaluation of ANTs 622 similarity metric performance in brain image registration. Neuroimage 54:2033-2044. 623 Bailus BJ, Pyles B, McAlister MM, O'Geen H, Lockwood SH, Adams AN, Nguyen JT, Yu A, Berman 624 RF, Segal DJ (2016) Protein Delivery of an Artificial Transcription Factor Restores Widespread 625 Ube3a Expression in an Angelman Syndrome Mouse Brain. Mol Ther 24:548-555. 626 Berg EL, Ching TM, Bruun DA, Rivera JK, Careaga M, Ellegood J, Lerch JP, Wöhr M, Lein PJ, 627 Silverman JL (2020a) Translational outcomes relevant to neurodevelopmental disorders 628 following early life exposure of rats to chlorpyrifos. J Neurodev Disord 12:40. 629 Berg EL, Pedersen LR, Pride MC, Petkova SP, Patten KT, Valenzuela AE, Wallis C, Bein KJ, Wexler A, 630 Lein PJ, Silverman JL (2020b) Developmental exposure to near roadway pollution produces 631 behavioral phenotypes relevant to neurodevelopmental disorders in juvenile rats. Transl 632 Psychiatry 10:289. 633 Berg EL, Copping NA, Rivera JK, Pride MC, Careaga M, Bauman MD, Berman RF, Lein PJ, Harony-634 Nicolas H, Buxbaum JD, Ellegood J, Lerch JP, Wöhr M, Silverman JL (2018) Developmental 635 social communication deficits in the Shank3 rat model of phelan-mcdermid syndrome and autism 636 spectrum disorder. Autism Res 11:587-601. 637 Berg EL et al. (2020c) Translational outcomes in a full gene deletion of ubiquitin protein ligase E3A rat 638 model of Angelman syndrome. Transl Psychiatry 10:39. 639 Berridge KC (2009) 'Liking' and 'wanting' food rewards: brain substrates and roles in eating disorders. 640 Physiol Behav 97:537-550. 641 Berridge KC, Aldridge JW (2009) Decision Utility, Incentive Salience, and Cue-Triggered "Wanting". 642 Oxf Ser Soc Cogn Soc Neurosci 2009:509-533. 643 Berridge KC, Robinson TE, Aldridge JW (2009) Dissecting components of reward: 'liking', 'wanting', and 644 learning. Curr Opin Pharmacol 9:65-73. 645 Bird LM (2014) Angelman syndrome: review of clinical and molecular aspects. Appl Clin Genet 7:93-

104.

Bishop J, Feintuch A, Bock NA, Nieman B, Dazai J, Davidson L, Henkelman RM (2006) Retrospective
gating for mouse cardiac MRI. Magn Reson Med 55:472-477.

Blanchard RJ, Blanchard DC, Agullana R, Weiss SM (1991) Twenty-two kHz alarm cries to presentation
of a predator, by laboratory rats living in visible burrow systems. Physiol Behav 50:967-972.

- Bock NA, Nieman BJ, Bishop JB, Mark Henkelman R (2005) In vivo multiple-mouse MRI at 7 Tesla.
  Magn Reson Med 54:1311-1316.
- Born HA, Dao AT, Levine AT, Lee WL, Mehta NM, Mehra S, Weeber EJ, Anderson AE (2017) Straindependence of the Angelman Syndrome phenotypes in Ube3a maternal deficiency mice. Sci Rep
  7:8451.
- Braun MD, Kisko TM, Vecchia DD, Andreatini R, Schwarting RKW, Wöhr M (2018) Sex-specific
  effects of Cacna1c haploinsufficiency on object recognition, spatial memory, and reversal
  learning capabilities in rats. Neurobiology of learning and memory 155:543-555.
- Bredewold R, Nascimento NF, Ro GS, Cieslewski SE, Reppucci CJ, Veenema AH (2018) Involvement of
  dopamine, but not norepinephrine, in the sex-specific regulation of juvenile socially rewarding
  behavior by vasopressin. Neuropsychopharmacology 43:2109-2117.
- Brudzynski SM (2009) Communication of adult rats by ultrasonic vocalization: biological,
   sociobiological, and neuroscience approaches. ILAR J 50:43-50.
- Brudzynski SM (2013) Ethotransmission: communication of emotional states through ultrasonic
  vocalization in rats. Curr Opin Neurobiol 23:310-317.
- Brudzynski SM (2015) Pharmacology of Ultrasonic Vocalizations in adult Rats: Significance, Call
  Classification and Neural Substrate. Curr Neuropharmacol 13:180-192.
- 668 Burgdorf J, Panksepp J (2001) Tickling induces reward in adolescent rats. Physiol Behav 72:167-173.
- Burgdorf J, Panksepp J, Brudzynski SM, Kroes R, Moskal JR (2005) Breeding for 50-kHz positive
  affective vocalization in rats. Behav Genet 35:67-72.

Burgdorf J, Kroes RA, Moskal JR, Pfaus JG, Brudzynski SM, Panksepp J (2008) Ultrasonic vocalizations
of rats (Rattus norvegicus) during mating, play, and aggression: Behavioral concomitants,
relationship to reward, and self-administration of playback. J Comp Psychol 122:357-367.

Burgdorf JS, Brudzynski SM, Moskal JR (2020) Using rat ultrasonic vocalization to study the
neurobiology of emotion: from basic science to the development of novel therapeutics for
affective disorders. Curr Opin Neurobiol 60:192-200.

Burke CJ, Kisko TM, Swiftwolfe H, Pellis SM, Euston DR (2017) Specific 50-kHz vocalizations are
tightly linked to particular types of behavior in juvenile rats anticipating play. PLoS One
12:e0175841.

Cassidy SB, Dykens E, Williams CA (2000) Prader-Willi and Angelman syndromes: sister imprinted
 disorders. Am J Med Genet 97:136-146.

682 Ciarlone SL, Grieco JC, D'Agostino DP, Weeber EJ (2016) Ketone ester supplementation attenuates
 683 seizure activity, and improves behavior and hippocampal synaptic plasticity in an Angelman
 684 syndrome mouse model. Neurobiol Dis 96:38-46.

Ciarlone SL, Wang X, Rogawski MA, Weeber EJ (2017) Effects of the synthetic neurosteroid ganaxolone
 on seizure activity and behavioral deficits in an Angelman syndrome mouse model.
 Neuropharmacology 116:142-150.

Collingridge GL, Isaac JT (2003) Functional roles of protein interactions with AMPA and kainate
 receptors. Neurosci Res 47:3-15.

Collins DL, Neelin P, Peters TM, Evans AC (1994) Automatic 3D intersubject registration of MR
 volumetric data in standardized Talairach space. J Comput Assist Tomogr 18:192-205.

692 Copping, Silverman (2020) Abnormal electrophysiological phenotypes and sleep deficits in a mouse
 693 model of Angelman Syndrome. Molecular Autism In press.

Copping NA, Silverman JL (2021) Abnormal electrophysiological phenotypes and sleep deficits in a
 mouse model of Angelman Syndrome. Mol Autism 12:9.

Copping NA, Christian SGB, Ritter DJ, Islam MS, Buscher N, Zolkowska D, Pride MC, Berg EL,
LaSalle JM, Ellegood J, Lerch JP, Reiter LT, Silverman JL, Dindot SV (2017) Neuronal
overexpression of Ube3a isoform 2 causes behavioral impairments and neuroanatomical
pathology relevant to 15q11.2-q13.3 duplication syndrome. Hum Mol Genet 26:3995-4010.

Daily JL, Nash K, Jinwal U, Golde T, Rogers J, Peters MM, Burdine RD, Dickey C, Banko JL, Weeber
 EJ (2011) Adeno-associated virus-mediated rescue of the cognitive defects in a mouse model for
 Angelman syndrome. PLoS One 6:e27221.

Dodge A, Peters MM, Greene HE, Dietrick C, Botelho R, Chung D, Willman J, Nenninger AW, Ciarlone
S, Kamath SG, Houdek P, Sumova A, Anderson AE, Dindot SV, Berg EL, O'Geen H, Segal DJ,
Silverman JL, Weeber EJ, Nash KR (2020) Generation of a Novel Rat Model of Angelman
Syndrome with a Complete Ube3a Gene Deletion. Autism Res 13:397-409.

Dorr AE, Lerch JP, Spring S, Kabani N, Henkelman RM (2008) High resolution three-dimensional brain
atlas using an average magnetic resonance image of 40 adult C57Bl/6J mice. Neuroimage 42:6069.

# Dutta R, Crawley JN (2020) Behavioral Evaluation of Angelman Syndrome Mice at Older Ages. Neuroscience 445:163-171.

- Egawa K, Kitagawa K, Inoue K, Takayama M, Takayama C, Saitoh S, Kishino T, Kitagawa M, Fukuda A
  (2012) Decreased tonic inhibition in cerebellar granule cells causes motor dysfunction in a mouse
  model of Angelman syndrome. Sci Transl Med 4:163ra157.
- Ellenbroek B, Youn J (2016) Rodent models in neuroscience research: is it a rat race? Dis Model Mech
  9:1079-1087.
- Fendt M, Brosch M, Wernecke KEA, Willadsen M, Wöhr M (2018) Predator odour but not TMT induces
  22-kHz ultrasonic vocalizations in rats that lead to defensive behaviours in conspecifics upon
  replay. Scientific reports 8:11041.
- Fernandez M, Mollinedo-Gajate I, Penagarikano O (2018) Neural Circuits for Social Cognition:
  Implications for Autism. Neuroscience 370:148-162.

Filonova I, Trotter JH, Banko JL, Weeber EJ (2014) Activity-dependent changes in MAPK activation in
 the Angelman Syndrome mouse model. Learn Mem 21:98-104.

Genovese CR, Lazar NA, Nichols T (2002) Thresholding of statistical maps in functional neuroimaging
using the false discovery rate. NeuroImage 15:870-878.

Gentile JK, Tan WH, Horowitz LT, Bacino CA, Skinner SA, Barbieri-Welge R, Bauer-Carlin A, Beaudet
 AL, Bichell TJ, Lee HS, Sahoo T, Waisbren SE, Bird LM, Peters SU (2010) A
 neurodevelopmental survey of Angelman syndrome with genotype-phenotype correlations. J Dev
 Behav Pediatr 31:592-601.

Grieco JC, Gouelle A, Weeber EJ (2018) Identification of spatiotemporal gait parameters and pressurerelated characteristics in children with Angelman syndrome: A pilot study. J Appl Res Intellect
Disabil 31:1219-1224.

Hammerschmidt K, Reisinger E, Westekemper K, Ehrenreich L, Strenzke N, Fischer J (2012) Mice do
not require auditory input for the normal development of their ultrasonic vocalizations. BMC
Neurosci 13:40.

Harony-Nicolas H, Kay M, du Hoffmann J, Klein ME, Bozdagi-Gunal O, Riad M, Daskalakis NP, Sonar
S, Castillo PE, Hof PR, Shapiro ML, Baxter MG, Wagner S, Buxbaum JD (2017) Oxytocin
improves behavioral and electrophysiological deficits in a novel Shank3-deficient rat. Elife 6.

Hofer MA, Shair H (1978) Ultrasonic vocalization during social interaction and isolation in 2-weeek-old
rats. Dev Psychobiol 11:495-504.

Hofer MA, Shair HN, Brunelli SA (2002) Ultrasonic vocalizations in rat and mouse pups. Current
 protocols in neuroscience / editorial board, Jacqueline N Crawley [et al] Chapter 8:Unit 8 14.

Homberg JR, Wöhr M, Alenina N (2017) Comeback of the Rat in Biomedical Research. ACS Chem
Neurosci 8:900-903.

Huang HS, Burns AJ, Nonneman RJ, Baker LK, Riddick NV, Nikolova VD, Riday TT, Yashiro K,
Philpot BD, Moy SS (2013) Behavioral deficits in an Angelman syndrome model: effects of
genetic background and age. Behav Brain Res 243:79-90.

Ishiyama S, Brecht M (2016) Neural correlates of ticklishness in the rat somatosensory cortex. Science
354:757-760.

# Jamal I, Kumar V, Vatsa N, Shekhar S, Singh BK, Sharma A, Jana NR (2017) Rescue of altered HDAC activity recovers behavioural abnormalities in a mouse model of Angelman syndrome. Neurobiol Dis 105:99-108.

Jiang YH, Armstrong D, Albrecht U, Atkins CM, Noebels JL, Eichele G, Sweatt JD, Beaudet AL (1998)
 Mutation of the Angelman ubiquitin ligase in mice causes increased cytoplasmic p53 and deficits
 of contextual learning and long-term potentiation. Neuron 21:799-811.

Jiang YH, Pan Y, Zhu L, Landa L, Yoo J, Spencer C, Lorenzo I, Brilliant M, Noebels J, Beaudet AL
(2010) Altered ultrasonic vocalization and impaired learning and memory in Angelman syndrome
mouse model with a large maternal deletion from Ube3a to Gabrb3. PLoS One 5:e12278.

- Judson MC, Burette AC, Thaxton CL, Pribisko AL, Shen MD, Rumple AM, Del Cid WA, Paniagua B,
  Styner M, Weinberg RJ, Philpot BD (2017) Decreased Axon Caliber Underlies Loss of Fiber
  Tract Integrity, Disproportional Reductions in White Matter Volume, and Microcephaly in
  Angelman Syndrome Model Mice. J Neurosci 37:7347-7361.
- Judson MC, Wallace ML, Sidorov MS, Burette AC, Gu B, van Woerden GM, King IF, Han JE, Zylka
  MJ, Elgersma Y, Weinberg RJ, Philpot BD (2016) GABAergic Neuron-Specific Loss of Ube3a
  Causes Angelman Syndrome-Like EEG Abnormalities and Enhances Seizure Susceptibility.
  Neuron 90:56-69.
- Kaphzan H, Hernandez P, Jung JI, Cowansage KK, Deinhardt K, Chao MV, Abel T, Klann E (2012)
  Reversal of impaired hippocampal long-term potentiation and contextual fear memory deficits in
  Angelman syndrome model mice by ErbB inhibitors. Biol Psychiatry 72:182-190.

Kisko TM, Euston DR, Pellis SM (2015) Are 50-khz calls used as play signals in the playful interactions
of rats? III. The effects of devocalization on play with unfamiliar partners as juveniles and as
adults. Behav Processes 113:113-121.

773 Kisko TM, Wöhr M, Pellis VC, Pellis SM (2017) From Play to Aggression: High-Frequency 50-kHz 774 Ultrasonic Vocalizations as Play and Appeasement Signals in Rats. Curr Top Behav Neurosci 775 30:91-108. 776 Kisko TM, Braun MD, Michels S, Witt SH, Rietschel M, Culmsee C, Schwarting RKW, Wöhr M (2018a) 777 Cacnalc haploinsufficiency leads to pro-social 50-kHz ultrasonic communication deficits in rats. 778 Disease models & mechanisms 11. 779 Kisko TM, Braun MD, Michels S, Witt SH, Rietschel M, Culmsee C, Schwarting RKW, Wöhr M (2018b) 780 Sex-dependent effects of Cacnalc haploinsufficiency on juvenile social play behavior and pro-781 social 50-kHz ultrasonic communication in rats. Genes Brain Behav:e12552. 782 Kondrakiewicz K, Kostecki M, Szadzinska W, Knapska E (2019) Ecological validity of social interaction 783 tests in rats and mice. Genes Brain Behav 18:e12525. 784 Ku CS, Loy EY, Pawitan Y, Chia KS (2010) The pursuit of genome-wide association studies: where are 785 we now? J Hum Genet 55:195-206. 786 Ku KM, Weir RK, Silverman JL, Berman RF, Bauman MD (2016) Behavioral Phenotyping of Juvenile 787 Long-Evans and Sprague-Dawley Rats: Implications for Preclinical Models of Autism Spectrum 788 Disorders. PLoS One 11:e0158150. 789 Kumar V, Joshi T, Vatsa N, Singh BK, Jana NR (2019) Simvastatin Restores HDAC1/2 Activity and

790 Improves Behavioral Deficits in Angelman Syndrome Model Mouse. Front Mol Neurosci 12:1-791 11.

Leach PT, Crawley JN (2018) Touchscreen learning deficits in Ube3a, Ts65Dn and Mecp2 mouse models
 of neurodevelopmental disorders with intellectual disabilities. Genes Brain Behav 17:e12452.

Lerch JP, Sled JG, Henkelman RM (2011) MRI phenotyping of genetically altered mice. Methods Mol
 Biol 711:349-361.

Lerch JP, Carroll JB, Spring S, Bertram LN, Schwab C, Hayden MR, Henkelman RM (2008a) Automated
 deformation analysis in the YAC128 Huntington disease mouse model. NeuroImage 39:32-39.

Lerch JP, Pruessner J, Zijdenbos AP, Collins DL, Teipel SJ, Hampel H, Evans AC (2008b) Automated
 cortical thickness measurements from MRI can accurately separate Alzheimer's patients from
 normal elderly controls. Neurobiol Aging 29:23-30.

# Lerch JP, Carroll JB, Dorr A, Spring S, Evans AC, Hayden MR, Sled JG, Henkelman RM (2008c) Cortical thickness measured from MRI in the YAC128 mouse model of Huntington's disease. NeuroImage 41:243-251.

Lopuch S, Popik P (2011) Cooperative behavior of laboratory rats (Rattus norvegicus) in an instrumental
 task. J Comp Psychol 125:250-253.

Meaney MJ, Stewart J (1981) Neonatal-androgens influence the social play of prepubescent rats.
Hormones and behavior 15:197-213.

- Meng L, Ward AJ, Chun S, Bennett CF, Beaudet AL, Rigo F (2015) Towards a therapy for Angelman
  syndrome by targeting a long non-coding RNA. Nature 518:409-412.
- 810 Netser S, Meyer A, Magalnik H, Zylbertal A, de la Zerda SH, Briller M, Bizer A, Grinevich V, Wagner S
- 811 (2020) Distinct dynamics of social motivation drive differential social behavior in laboratory rat
  812 and mouse strains. Nat Commun 11:5908.
- Nieman BJ, Shyu JY, Rodriguez JJ, Garcia AD, Joyner AL, Turnbull DH (2010) In vivo MRI of neural
  cell migration dynamics in the mouse brain. NeuroImage 50:456-464.
- 815 Nieman BJ, van Eede MC, Spring S, Dazai J, Henkelman RM, Lerch JP (2018) MRI to Assess
- 816 Neurological Function. Curr Protoc Mouse Biol 8:e44.
- 817 Okabe S, Takayanagi Y, Yoshida M, Onaka T (2021) Post-weaning stroking stimuli induce affiliative
  818 behavior toward humans and influence brain activity in female rats. Sci Rep 11:3805.
- 819 Panksepp J (1981) The ontogeny of play in rats. Dev Psychobiol 14:327-332.
- 820 Panksepp J (2005) Psychology. Beyond a joke: from animal laughter to human joy? Science 308:62-63.
- 821 Panksepp J, Beatty WW (1980) Social deprivation and play in rats. Behav Neural Biol 30:197-206.

825

Panksepp J, Burgdorf J (2000) 50-kHz chirping (laughter?) in response to conditioned and unconditioned
tickle-induced reward in rats: effects of social housing and genetic variables. Behav Brain Res
115:25-38.

Parker CC, Chen H, Flagel SB, Geurts AM, Richards JB, Robinson TE, Solberg Woods LC, Palmer AA

# (2014) Rats are the smart choice: Rationale for a renewed focus on rats in behavioral genetics. Neuropharmacology 76 Pt B:250-258.

- Pellis SM, Pellis VC (1998) Play fighting of rats in comparative perspective: a schema for
   neurobehavioral analyses. Neuroscience and biobehavioral reviews 23:87-101.
- 830 Pellis SM, Pellis VC (2017) What is play fighting and what is it good for? Learn Behav 45:355-366.

Portfors CV (2007) Types and functions of ultrasonic vocalizations in laboratory rats and mice. J Am
Assoc Lab Anim Sci 46:28-34.

- Portfors CV, Perkel DJ (2014) The role of ultrasonic vocalizations in mouse communication. Curr Opin
  Neurobiol 28:115-120.
- Powell E, Anch AM, Dyche J, Bloom C, Richtert RR (1999) The splay angle: A new measure for
  assessing neuromuscular dysfunction in rats. Physiol Behav 67:819-821.
- Reppucci CJ, Brown LA, Chambers AQ, Veenema AH (2020) Wistar rats and C57BL/6 mice differ in
  their motivation to seek social interaction versus food in the Social versus Food Preference Test.
  Physiol Behav 227:113162.
- 840 Rygula R, Pluta H, Popik P (2012) Laughing rats are optimistic. PloS one 7:e51959.
- Sadananda M, Wöhr M, Schwarting RK (2008) Playback of 22-kHz and 50-kHz ultrasonic vocalizations
  induces differential c-fos expression in rat brain. Neurosci Lett 435:17-23.
- Schwarting RK, Jegan N, Wöhr M (2007) Situational factors, conditions and individual variables which
  can determine ultrasonic vocalizations in male adult Wistar rats. Behav Brain Res 182:208-222.
- Spencer Noakes TL, Henkelman RM, Nieman BJ (2017) Partitioning k-space for cylindrical threedimensional rapid acquisition with relaxation enhancement imaging in the mouse brain. NMR
  Biomed 30.

Steadman PE, Ellegood J, Szulc KU, Turnbull DH, Joyner AL, Henkelman RM, Lerch JP (2014) Genetic
effects on cerebellar structure across mouse models of autism using a magnetic resonance
imaging atlas. Autism Res 7:124-137.

Tan WH, Bird LM (2016) Angelman syndrome: Current and emerging therapies in 2016. Am J Med
Genet C Semin Med Genet 172:384-401.

Tan WH, Bacino CA, Skinner SA, Anselm I, Barbieri-Welge R, Bauer-Carlin A, Beaudet AL, Bichell TJ,
Gentile JK, Glaze DG, Horowitz LT, Kothare SV, Lee HS, Nespeca MP, Peters SU, Sahoo T,
Sarco D, Waisbren SE, Bird LM (2011) Angelman syndrome: Mutations influence features in
early childhood. Am J Med Genet A 155A:81-90.

van Woerden GM, Harris KD, Hojjati MR, Gustin RM, Qiu S, de Avila Freire R, Jiang YH, Elgersma Y,
Weeber EJ (2007) Rescue of neurological deficits in a mouse model for Angelman syndrome by
reduction of alphaCaMKII inhibitory phosphorylation. Nat Neurosci 10:280-282.

Varlinskaya EI, Spear LP (2008) Social interactions in adolescent and adult Sprague-Dawley rats: impact
of social deprivation and test context familiarity. Behav Brain Res 188:398-405.

862 Weeber EJ, Jiang YH, Elgersma Y, Varga AW, Carrasquillo Y, Brown SE, Christian JM, Mirnikjoo B,

863 Silva A, Beaudet AL, Sweatt JD (2003) Derangements of hippocampal calcium/calmodulin864 dependent protein kinase II in a mouse model for Angelman mental retardation syndrome. J
865 Neurosci 23:2634-2644.

Wheeler AC, Sacco P, Cabo R (2017) Unmet clinical needs and burden in Angelman syndrome: a review
of the literature. Orphanet J Rare Dis 12:164.

Williams C, Franco L (2010) Angelman syndrome at the synapse: meeting report of the Angelman
Syndrome Foundation's 2009 scientific symposium. J Child Neurol 25:254-261.

870 Williams CA (2005) Neurological aspects of the Angelman syndrome. Brain Dev 27:88-94.

Williams CA (2010) The behavioral phenotype of the Angelman syndrome. Am J Med Genet C Semin
Med Genet 154C:432-437.

873 Willuhn I, Tose A, Wanat MJ, Hart AS, Hollon NG, Phillips PE, Schwarting RK, Wöhr M (2014) Phasic

- dopamine release in the nucleus accumbens in response to pro-social 50 kHz ultrasonic
  vocalizations in rats. J Neurosci 34:10616-10623.
- 876 Wöhr M (2021) Measuring mania-like elevated mood through amphetamine-induced 50-kHz ultrasonic
- 877 vocalizations in rats. Br J Pharmacol 2021:1-19.
- Wöhr M, Houx B, Schwarting RK, Spruijt B (2008) Effects of experience and context on 50-kHz
  vocalizations in rats. Physiol Behav 93:766-776.
- Wöhr M, Schwarting RK (2007) Ultrasonic communication in rats: can playback of 50-kHz calls induce
  approach behavior? PLoS One 2:e1365.
- Wöhr M, Schwarting RK (2013) Affective communication in rodents: ultrasonic vocalizations as a tool
  for research on emotion and motivation. Cell and tissue research 354:81-97.
- Wöhr M, Seffer D, Schwarting RK (2016) Studying Socio-Affective Communication in Rats through
  Playback of Ultrasonic Vocalizations. Curr Protoc Neurosci 75:8 35 31-38 35 17.
- Wöhr M, Kehl M, Borta A, Schanzer A, Schwarting RK, Hoglinger GU (2009) New insights into the
  relationship of neurogenesis and affect: tickling induces hippocampal cell proliferation in rats
  emitting appetitive 50-kHz ultrasonic vocalizations. Neuroscience 163:1024-1030.
- 889 Wolter JM, Mao H, Fragola G, Simon JM, Krantz JL, Bazick HO, Oztemiz B, Stein JL, Zylka MJ (2020)
- 890 Cas9 gene therapy for Angelman syndrome traps Ube3a-ATS long non-coding RNA. Nature
- 891
   587:281-284.
- 892 Zucker RS (1989) Short-term synaptic plasticity. Annu Rev Neurosci 12:13-31.
- 893 Zucker RS, Regehr WG (2002) Short-term synaptic plasticity. Annu Rev Physiol 64:355-405.
- 894

### 895 Data Availability

896 Data are available from the corresponding author upon request.

897

### 898 Figure Legends

899

900 **Figure 1.** Overabundant emission of laughter-like 50-kHz calls in juvenile  $Ube3a^{\text{mat-/pat+}}$  rats. (A) 901 Example images of the manipulations used to mimic social play and elicit ultrasonic vocalizations (USV). 902 (B) Example spectrograms of USV from a wildtype littermate control ( $Ube3a^{mat+/pat+}$ ; mat+/pat+; upper) 903 and Ube3a<sup>mat-/pat+</sup> rat (mat-/pat+; lower). (C) Across five days of heterospecific play sessions, 50-kHz 904 USV emission increased with repeated testing in both mat-/pat+ (n=25) and controls (n=25), but the 905 emission rate was substantially elevated in mat-/pat+. (D) On average, mat-/pat+ rats produced 50-kHz 906 USV at more than twice the rate of controls. (E) Specifically, 50-kHz calling was abnormally high during 907 the break and belly tickle phases, with trending increases during neck tickle, push and drill, and flip over. 908 (F) Prior to the onset of play, mat-/pat+ rats emitted anticipatory 50-kHz USV at more than three times 909 the rate of controls. (G) Production of short 22-kHz USV was low, did not differ between genotypes, and 910 did not change over subsequent play sessions. (H) The rates of 50-kHz and short 22-kHz calling during 911 empty cage exploration were comparable between genotypes (mat+/pat+, n=32; mat-/pat+, n=29), as were 912 the (I) 50-kHz and short 22-kHz calling rates in response to hearing playback of conspecific 50-kHz USV 913 (mat+/pat+, n=9; mat-/pat+, n=12). Call features did not differ by genotype: (J) The average duration and 914 (K) peak frequency of spontaneous 50-kHz calls made during exploration of an empty cage was 915 comparable between mat-/pat+ (n=23) and mat+/pat+ rats (n=25). (L) The average duration and (M) 916 average peak frequency of short 22-kHz calls made within an empty cage were also similar between 917 genotypes (mat+/pat+, n=6; mat-/pat+, n=7). (N) For 50-kHz USV emitted in response to hearing 918 playback of natural pre-recorded 50-kHz rat USV, average duration and (O) average peak frequency were 919 comparable between mat-/pat+ rats (n=12) and wildtype littermates (n=9). (P) There was no genotype 920 effect on the average duration or (Q) average peak frequency of short 22-kHz calls made during USV 921 playback (mat+/pat+, n=3; mat-/pat+, n=2). Of note, long 22-kHz USV known to function as "alarm

calls" were very rarely observed, indicating that our paradigms were not aversive. Data are depicted as mean  $\pm$  S.E.M. C: \*\*p<0.01, repeated measures ANOVA. D, F: \*\*\*p<0.001, \*\*p<0.01, Mann-Whitney test. E: \*p<0.05, \*p<0.06, repeated measures ANOVA, Holm-Sidak's *post-hoc*.

925

926 Figure 2. Intact social interest but deficient expression of key social interaction behaviors in juvenile Ube3a<sup>mat-/pat+</sup> rats. (A) During a 10-min interaction session with a novel same-sex wildtype conspecific, 927 Ube3a<sup>mat-/pat+</sup> rats (mat-/pat+; n=12) spent similar amounts of time social sniffing, (B) anogenital sniffing, 928 929 (C) self-grooming, and (D) exploring the arena compared to wildtype littermate controls (Ube3a<sup>mat+/pat+</sup>; 930 mat+/pat+; n=10). (E) Robust deficits, however, were discovered in the time spent following or chasing 931 and (F) rough-and-tumble playing. (G) The number of push pasts were similar across genotypes but (H) 932 there was a trend for mat-/pat+ to less frequently push under or crawl over and (I) mat-/pat+ rats did not 933 perform nearly as many pounces as wildtype littermates. (J) A separate test of olfactory discrimination 934 revealed normal sniff times of social and non-social scents. Time spent investigating novel odors was 935 similar for mat-/pat+ (n=7) and mat+/pat+ rats (n=7) and both groups spent more time investigating a social scent compared to a non-social vanilla odor. Data are depicted as mean  $\pm$  S.E.M. E-I: \*\*p<0.01, 936 937 \*p<0.05, <sup>#</sup>p<0.065, Mann-Whitney test. J: \*p<0.05, repeated measures ANOVA, Holm-Sidak's post-hoc. 938

Figure 3. Abnormal gait in Ube3a<sup>mat-/pat+</sup> rats. (A) While treadmill walking, Ube3a<sup>mat-/pat+</sup> rats (mat-/pat+; 939 940 n=23) displayed aberrant propulsion time (time from maximal paw contact with belt to just before liftoff) 941 in both sets of limbs. Compared to wildtype littermates ( $Ube3a^{mat+/pat+}$ ; mat+/pat+; n=23), propulsion time 942 was decreased in the forelimbs and increased in hindlimbs. (B) Brake time (time from initial to maximal 943 paw contact with belt) was significantly elevated in the forelimbs of mat-/pat+ while a trending reduction 944 in hindlimb brake time was found (p=0.150). (C) Swing time (no paw contact with the belt) and (D) stride 945 time (sum of swing and stance time) were similar across genotypes. (E) Example paw prints illustrating 946 the spatial gait parameters depicted in panels F, G, and H. (F) Stride length did not differ between groups, 947 but (G) forelimb stance width was narrower and (H) absolute paw angle for the forelimbs was greater,

948 indicating more external rotation in mat-/pat+ rats. (I) No significant difference in gait symmetry (ratio of
949 forelimb to hindlimb stepping frequency) was detected. Data are depicted as mean ± S.E.M. \*\*p<0.01,</li>
950 \*p<0.05, repeated measures ANOVA, Holm-Sidak's *post-hoc*.

951

Figure 4. Impaired learning and memory in Ube3a<sup>mat-/pat+</sup> rats. (A) During fear conditioning training, 952 953 juvenile  $Ube3a^{\text{mat-/pat+}}$  (mat-/pat+; n=12) and wildtype littermate controls ( $Ube3a^{\text{mat-/pat+}}$ ; mat+/pat+; n=20) 954 showed similar increases in freezing post-training. (B) When returned to the training context 24 hrs 955 following training, mat-/pat+ rats exhibited a similar level of freezing to wildtypes. (C) When introduced 956 to a novel context 48 hrs after training, no difference in freezing pre-cue was found but mat-/pat+ rats 957 froze for less than half the time of wildtypes during presentation of the auditory cue. A separate 958 sensorimotor test confirmed intact auditory sensitivity: (D) Baseline activity within the testing apparatus 959 was comparable between mat-/pat+ (n=10) and mat+/pat+ rats (n=14). (E) There was no effect of 960 genotype on the startle response to a 120 decibel (dB) startle stimulus. (F) Prepulse inhibition of the 961 startle response was generally reduced in adult mat-/pat+ rats. (G) Spontaneous arm alternation during Y-962 maze exploration was significantly reduced in adult mat-/pat+ rats (n=24) compared to wildtype 963 littermates (n=24). (H) Mat-/pat+ rats made 40% more errors and (I) made more entries into the maze 964 arms. Bars indicate mean ± S.E.M. A, C: \*\*\*\*p<0.0001, \*\*\*p<0.001, repeated measures ANOVA, 965 Holm-Sidak's post-hoc. F: \*p<0.05, repeated measures ANOVA main effect. G-I: \*\*\*p<0.001, \*\*p<0.01, 966 Student's t-test.

967

Figure 5. Reduced hippocampal long-term potentiation (LTP) in  $Ube3a^{\text{mat-/pat+}}$  rats. (A) Normal basal synaptic transmission as measured by presynaptic fiber volley amplitudes and postsynaptic fEPSP slopes for responses elicited by different intensities of SC fiber stimulation in  $Ube3a^{\text{mat-/pat+}}$  (mat-/pat+; *n*=16) and wildtype littermate ( $Ube3a^{\text{mat+/pat+}}$ ; mat+/pat+; *n*=11) hippocampal slices. (B) Paired-pulse facilitation was unchanged at mat-/pat+ SC-CA1 synapses compared to mat+/pat+ (*n*=15 mat+/pat+ and *n*=20 mat-/pat+ slices). (Right) Traces represent fEPSPs evoked by stimulation pulses delivered with a 50 msec 974 interpulse interval. Scale bars: 0.5 mV, 25 msec. (C) High frequency stimulation (HFS)-induced LTP in 975 mat+/pat+ (n=11) was significantly greater compared to mat-/pat+ (n=16). Traces at right represent 976 superimposed fEPSPs recorded during baseline and 60 min after HFS. Scale bars: 1 mV, 5 msec. (D) 977 Summary graph of average percentage potentiation relative to baseline demonstrating that mat+/pat+ 978 exhibited significantly enhanced SC-CA1 LTP at 60 min after HFS (delivered at time = 0), fEPSPs were 979 potentiated to 160 ± 7% of baseline in mat+/pat+ (n=11) and were 127 ± 5% of baseline in mat-/pat+ 980 slices (n=16). Data were collected from two rats per genotype. \*\*\*\*p<0.0001, Student's *t*-test.

981

Figure 6. Neuroanatomical pathology in Ube3a<sup>mat-/pat+</sup> rats revealed by high-resolution magnetic 982 983 resonance imaging (MRI). (Left) Slice series comparing absolute volume (mm<sup>3</sup>) of juvenile and adult 984 populations of Ube3a<sup>mat-/pat+</sup> (mat-/pat+) rats and wildtype littermates (Ube3a<sup>mat+/pat+</sup>; mat+/pat+). Red to 985 yellow coloration indicates increased volume compared to wildtype whereas dark blue to light blue 986 indicates decreased volume. The leftmost column is data on juvenile mat-/pat+ rats from Berg et al. 987 (2020) and the center column illustrates the same slices on the adult dataset presented here. Most notably, 988 total brain volume was 6.0% smaller in mat-/pat+ rats compared to wildtype. Additionally, the third 989 column shows the genotype by age interaction highlighting several regions of interest, (right) four of 990 which are shown in panels A-D. Namely, (A) fiber tracts, (B) the hypothalamus, (C) the hippocampal 991 region, and (D) the thalamus. Full detail of regional findings for adult animals and the interaction effect 992 are described in Figures 6-1 and 6-2. Group sizes: juvenile mat+/pat, n=29; juvenile mat-/pat+, n=25; 993 adult mat+/pat+, n=23; adult mat-/pat+, n=24. Bars indicate mean ± S.E.M. \*\*\*\*p<0.0001, \*\*p<0.01, 994 two-way ANOVA, Holm-Sidak's post-hoc.

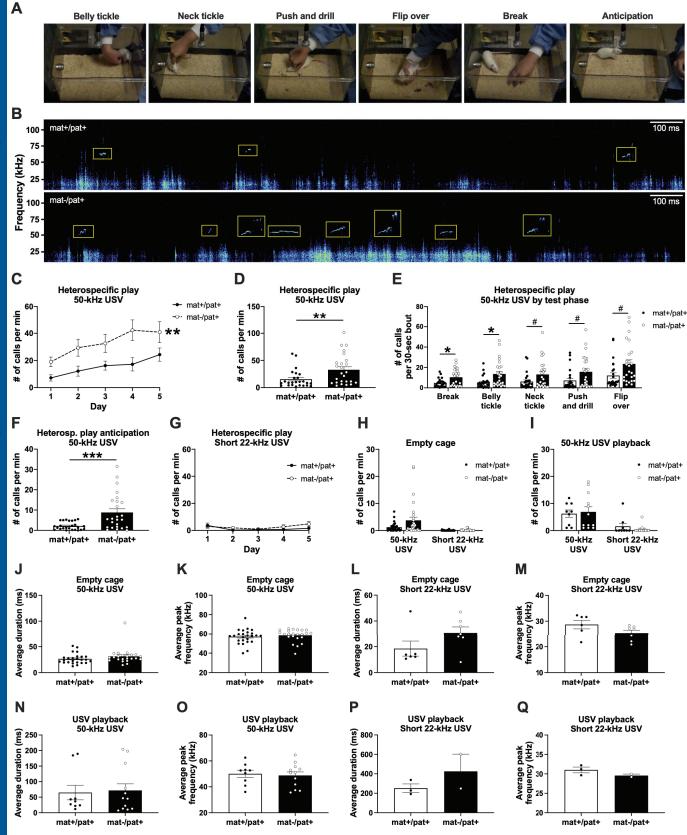
995

### 996 Extended Data Figure Legends

997

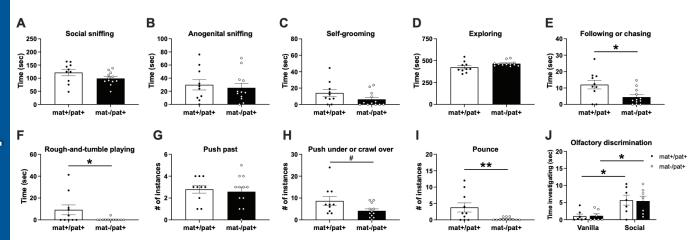
**Figure 6-1.** Brain volumes for adult *Ube3a*<sup>mat-/pat+</sup> rats and wildtype littermates.

- 1000 Figure 6-2. Age by genotype interaction for absolute brain volumes of juvenile and adult  $Ube3a^{\text{mat-/pat+}}$
- 1001 rats and wildtype littermates.

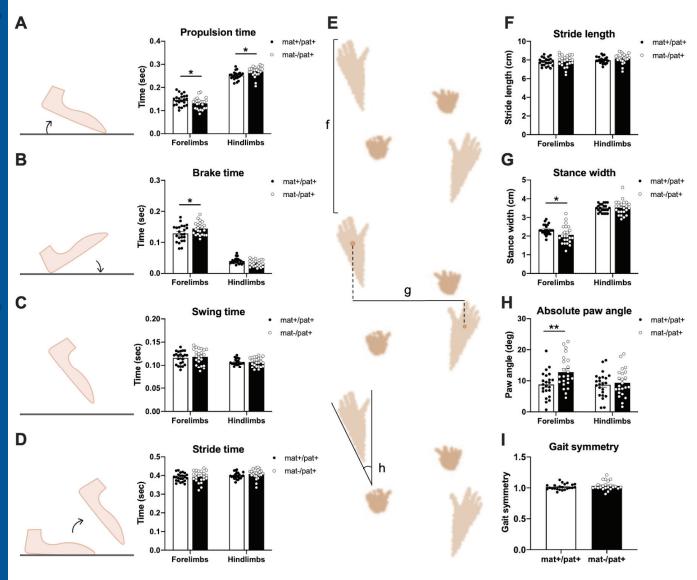


<u>JNeurosci Accepted Manuscript</u>

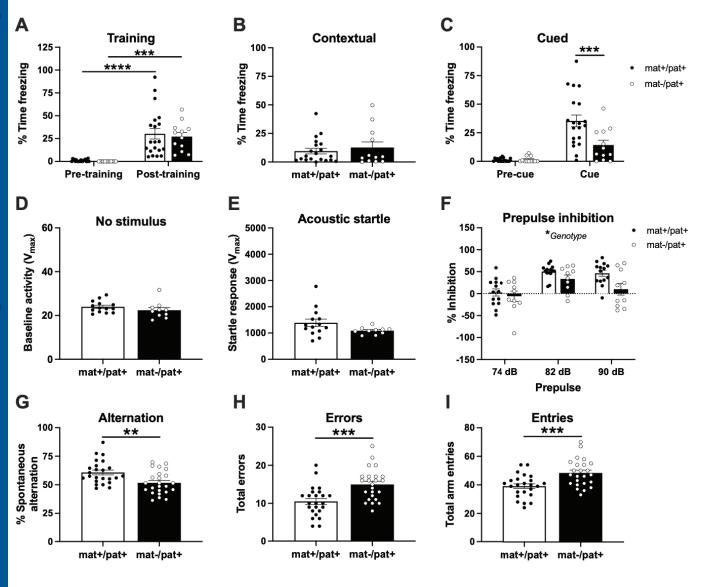
# **JNeurosci Accepted Manuscript**



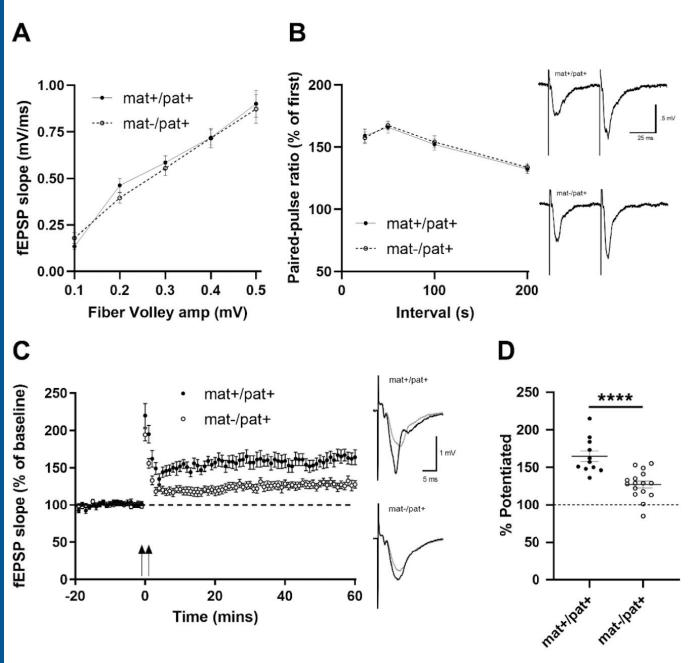












# **JNeurosci Accepted Manuscript**

